

The Growth of Massive Black Holes in Galaxy Merger Simulations with Feedback by Radiation Pressure

Jackson DeBuhr,^{1,2} Eliot Quataert,^{1,2} and Chung-Pei Ma²

¹*Department of Physics, University of California, Berkeley, CA 94720, USA*

²*Department of Astronomy and Theoretical Astrophysics Center, University of California, Berkeley, CA 94720, USA*

18 June 2010

ABSTRACT

We study the growth of massive black holes (BH) in galaxies using smoothed particle hydrodynamic simulations of major galaxy mergers with new implementations of BH accretion and feedback. The effect of BH accretion on gas in its host galaxy is modeled by depositing momentum at a rate $\sim \tau L/c$ into the ambient gas, where L is the luminosity produced by accretion onto the BH and τ is the wavelength-averaged optical depth of the galactic nucleus to the AGN’s radiation (a free parameter of our model). The accretion rate onto the BH is relatively independent of our subgrid accretion model and is instead determined by the BH’s dynamical impact on its host galaxy: BH accretion is thus self-regulated rather than “supply limited.” We show that the final BH mass and total stellar mass formed during a merger are more robust predictions of the simulations than the time dependence of the star formation rate or BH accretion rate. In particular, the latter depend on the assumed interstellar medium physics, which determines when and where the gas fragments to form star clusters; this in turn affects the fuel available for further star formation and BH growth. Simulations over a factor of ~ 30 in galaxy mass are consistent with the observed $M_{BH} - \sigma$ relation for a mean optical depth of $\tau \sim 25$. This requires that most BH growth occur when the galactic nucleus is optically thick to far-infrared radiation, consistent with the hypothesized connection between ultra-luminous infrared galaxies and quasars. We find tentative evidence for a shallower $M_{BH} - \sigma$ relation in the lowest mass galaxies, $\sigma \lesssim 100 \text{ km s}^{-1}$. Our results demonstrate that feedback-regulated BH growth and consistency with the observed $M_{BH} - \sigma$ relation do not require that BH feedback terminate star formation in massive galaxies or unbind large quantities of cold gas.

Key words: galaxies: evolution – galaxies: active

1 INTRODUCTION

Feedback from an active galactic nucleus (AGN) has been invoked to resolve a number of observational problems in galaxy formation: (1) to explain the tight observed (Ferrarese & Merritt 2000; Gebhardt et al. 2000; Häring & Rix 2004) correlations between central black hole (BH) and galaxy properties such as the $M_{BH} - \sigma$ and $M_{BH} - M_*$ relations and the BH “fundamental plane” (Silk & Rees 1998; King 2003; Murray et al. 2005; Di Matteo et al. 2005; Sazonov et al. 2005; Hopkins et al. 2007), (2) to shut off star formation in elliptical galaxies (e.g., by blowing gas out of the galaxy), thereby explaining how ellipticals become “red and dead” (e.g., Springel et al. 2005a; Ciotti et al. 2010), (3) to heat the hot intracluster plasma (ICM) in groups and clusters, thereby suppressing cooling and star formation in these environments (e.g., Tabor & Binney 1993; Ciotti & Ostriker 1997; Croton et al. 2006), and (4) to help explain “cosmic downsizing,” namely the fact that both star

formation and AGN activity reside in progressively lower mass halos at lower redshifts (e.g., Scannapieco et al. 2005).

It is plausible that AGN perform the roles desired of them, but this is by no means certain. Understanding whether this is indeed the case requires developing more sophisticated theoretical models that can be compared quantitatively to observations. There are several key theoretical problems that must be addressed in order to better understand the role of massive BHs in galaxy formation, and to understand the properties of massive BHs themselves. The first is the problem of AGN fueling, i.e., how is gas transferred from galactic scales ($\sim 0.1 - 1 \text{ kpc}$) to the vicinity of the massive BH ($\lesssim 0.1 \text{ pc}$)? A second key problem is the problem of AGN feedback: how do energy and momentum generated by accretion onto a central BH – in the form of radiation and outflows – couple to the surrounding gas, and how does this affect star formation and the growth of the BH itself?

Much of the recent work addressing the impact of BHs on galaxy formation has used qualitatively similar physics (e.g., Springel et al. 2005b; Johansson et al. 2009). For example, many calculations assume that a BH of mass M_{BH} will accrete mass at a rate proportional to the Bondi rate (Bondi 1952):

$$\dot{M}_{Bondi} = \frac{4\pi f G^2 M_{BH}^2 \rho}{c_s^3} \quad (1)$$

where ρ is the density of the surrounding gas, c_s is the sound speed of that gas, and $f \sim 10 - 100$ is a factor taking into account the possible multi-phase structure of the gas and that the sphere of influence of the BH is often not resolved (Booth & Schaye 2009). There is, however, little justification for using equation 1. The Bondi accretion rate estimate assumes that the gas surrounding the BH is spherically symmetric. When the gas is not spherically distributed, the rate of angular momentum transport determines the BH accretion rate (e.g., Shlosman et al. 1990). It is generally believed that the progenitors of today's $\gtrsim L^*$ ellipticals are gas-rich disk galaxies, the mergers of which lead to luminous starbursts and the growth of the central massive BHs (Sanders et al. 1988; Hopkins et al. 2005). Most of the gas in disk galaxies, merging galaxies, luminous starbursts (Downes & Solomon 1998; Tacconi et al. 2006), and nearby luminous AGN (Ho et al. 2008) appears to reside in a rotationally supported disk. There is thus no reason to expect that the spherically symmetric Bondi rate provides a good estimate of the BH accretion rate in gas rich galaxies. Even in the central \sim parsec of own galaxy, where the ambient gas *is* hot and pressure supported, the Bondi accretion rate fails by orders of magnitude to predict the accretion rate onto the central BH (Sharma et al. 2007).

There are a number of ways that an AGN can strongly influence its surroundings (e.g., Ostriker et al. 2010). Relativistic jets inject energy into intracluster plasma and may be the primary mechanism suppressing cooling flows in galaxy clusters (McNamara & Nulsen 2007), even though the details of how the energy in the jet couples to the plasma in a volume filling way are not fully understood (Vernaleo & Reynolds 2006). On galactic scales, a wind from an accretion disk around the BH can drive gas out of the galaxy (e.g., King 2003) as could cosmic-ray protons produced by a radio loud AGN (Sironi & Socrates 2010). In addition, the AGN's radiation can strongly affect the surrounding gas, both by Compton heating/cooling (e.g., Sazonov et al. 2005) and by the momentum imparted as UV radiation is absorbed by dust grains (Chang et al. 1987; Sanders et al. 1988; Murray et al. 2005).

This diversity of feedback mechanisms can be roughly separated into two broad classes: energy and momentum injection. We believe that momentum injection is the dominant mode of feedback for most of the gas in a galaxy, largely because of the very short cooling times of dense gas. For example, if a BH radiates at $\sim 10^{46}$ erg s $^{-1}$ with a typical quasar spectrum, only gas with $n \lesssim 1$ cm $^{-3}$ can be heated to the Compton temperature within ~ 100 pc. However, the mean gas densities in the central $\sim 0.1 - 1$ kpc of luminous star forming galaxies are $\sim 10^{3-5}$ cm $^{-3}$ (Downes & Solomon 1998; Tacconi et al. 2006). At these densities, the cooling time of gas is sufficiently short that it is unable to retain much injected energy – be it from the AGN's radiation or

from shocks powered by AGN outflows. Thus it is largely the momentum imparted by AGN outflows and by the absorption and scattering of the AGN's radiation that dominates the impact of the AGN on dense gas in galaxies. Since it is the dense gas that fuels star formation and the growth of the BH itself, it is critical to understand the impact of momentum feedback on this gas.¹

In this paper, we present simulations of major mergers of spiral galaxies using a model for the growth of BHs that includes (1) a BH accretion rate prescription motivated by the physics of angular momentum transport and (2) AGN feedback via momentum injection (e.g., radiation pressure). Some results of this model appear in a companion Letter (DeBuhr et al. 2009). The remainder of this paper is organized as follows. Section 2 presents a summary of our methods, including a description of the model galaxies (§2.1), the model for star formation and the interstellar medium (§2.2), our BH accretion and feedback model (§2.3) and a summary of our parameter choices (§2.4). Section 3 shows the results of applying this model to BH growth and star formation in major mergers of gas-rich galaxies. In section 4 we show that our model of BH growth and feedback produces a reasonably tight $M_{BH} - \sigma$ correlation similar to that observed. Finally, in section 5 we discuss our results and compare our approach to previous models in the literature. Appendix A presents resolution tests for our fiducial simulation while Appendix B presents some of the tests used to verify the BH accretion and feedback models that we have implemented.

2 METHODOLOGY

We use a non-public update of the TreeSPH code GADGET-2 (Springel 2005) provided by V. Springel to perform simulations of equal-mass mergers of galaxies. This version of the code includes the effective star formation model of Springel & Hernquist (2003) but contains no AGN feedback physics. We modified the code further to implement models for massive BH growth and AGN feedback. The details of the simulations are described in the following subsections. The Appendices present resolution tests and some of the tests we performed to verify our implementation of the BH accretion and feedback model.

2.1 Initial Conditions and Galaxy Parameters

Each model galaxy used in our major merger simulations is similar to those in Springel et al. (2005b). They include a spherical halo of collisionless dark matter, a centrifugally supported disk of gas and stars, a stellar bulge, and a central point mass representing a black hole. The code used to generate the initial conditions was provided by V. Springel and is identical to that used in Springel et al. (2005b) except for one change that will be described below.

Table 1 lists the relevant galaxy and simulation parameters for the key merger simulations we focus on in this paper. The simulations are all major mergers of equal mass galaxies. The fiducial simulation (top entry) assumes a mass of $1.94 \times 10^{12} M_\odot$ for each merging galaxy, of which 4.1% is

¹ These conclusions do not apply to dilute plasma in the intracluster or intragroup medium. The densities there are sufficiently low that the plasma can be efficiently heated by an AGN.

assigned to the gas and stars in the disk, 1.36% is assigned to the stars in the bulge, and the rest is in a dark matter halo. The initial mass fraction of gas in the disk is $f_g = 0.1$. This run uses a total of $N_p = 1.6 \times 10^6$ particles with 6×10^5 dark matter particles, 2×10^5 particles each in the gaseous and stellar disk, and 10^5 particles for the stellar bulge. This run has a Plummer equivalent gravitational force softening of $\epsilon = 47$ pc.

To test the dependence of the results of our fiducial simulation on the model and simulation parameters, we have run a number of additional simulations, varying the gas fraction ($f_g = 0.3$ vs 0.1), bulge-to-disk mass ratio (0.2 vs 0.33), total galaxy mass (from 0.1 to 3 of the fiducial value), simulation particle number (from $N_p = 1.6 \times 10^5$ to 2.4×10^6), force softening ($\epsilon = 22$ to 102 pc), as well as the parameters in the black hole model (described in § 2.4 below).

We use a Hernquist (1990) density profile for the structure of the dark matter halo:

$$\rho_{halo}(r) = \frac{M_{halo}}{2\pi} \frac{a}{r(r+a)^3}. \quad (2)$$

The scale length a of the halo is set by requiring that the halo enclose the same mass within the virial radius as an NFW profile, and that the densities match at small radii. These conditions yield a relationship among the halo scale length, a , the corresponding NFW scale length, r_s , and the concentration of the NFW halo, c (Navarro et al. 1996; Springel et al. 2005b): $a = r_s \{2[\ln(1+c) - c/(1+c)]\}^{1/2}$. The halos used in this work all have a concentration of $c = 9$.

The stellar and gaseous disks both initially have exponential surface density profiles:

$$\Sigma(R) = \frac{M_i}{2\pi R_d^2} \exp\left(-\frac{R}{R_d}\right) \quad (3)$$

where M_i is the total mass of the component of interest and R_d is the disk scale length, which is initially the same for the stellar and gaseous disks. The disk scale length for the fiducial simulation is $R_d = 3.5$ kpc, which corresponds to the disk having approximately the same angular momentum per unit mass as a halo with a spin parameter of 0.033. For simulations with different disk masses, we use $R_d \propto M_d^{1/3}$, which is consistent with the observed relation (Shen et al. 2003). The stellar disk’s vertical structure is given by the standard $\text{sech}^2(z/z_0)$ profile, where the vertical scale height z_0 is initially set to $z_0 = R_d/5$ at all radii. Unlike the stellar disk, the gaseous disk’s vertical structure is determined by hydrostatic equilibrium given the assumed sound speed/equation of state of the gas (discussed below). Setting up this initial vertical hydrostatic equilibrium requires an iterative procedure that is described in Springel et al. (2005b).

The stellar bulges also have Hernquist density profiles. The scale length of the bulge R_b is specified as a fraction of the disk scale length, R_d . In the fiducial simulation, $R_b = R_d/5$. For different bulge masses, we use the scaling relation $R_b \propto M_b^{1/2}$, which is motivated by the observed mass-radius relation of elliptical galaxies (Shen et al. 2003).

In our simulations, two galaxies with identical structure are placed on a prograde orbit. For simulations at our fiducial mass of $1.94 \times 10^{12} M_\odot$ (for each galaxy), the initial separation of the two galaxies’ centers is 142.8 kpc. The orbit has approximately zero total energy, which corresponds to an initial velocity for each galaxy of 160 km s^{-1} ; the ve-

locity is directed at an angle of 28 degrees from the line connecting the centers of the two galaxies. In order to break the symmetry of the problem, the individual spin axes of the galaxies have a relative angle of about 41 degrees, with one galaxy of the pair having an inclination with respect to the orbital plane of 10 degrees. For the simulations with different overall masses, the orbital parameters are scaled by $M^{1/3}$, so that the time to first passage and the time to final merger are similar to those in the fiducial run.

2.2 Interstellar Medium Model

The version of GADGET we use includes Springel & Hernquist (2003)’s sub-resolution model for the interstellar medium (ISM). This model treats the gas as a two phase medium of cold star forming clouds and a hot ISM. When cooling and star formation are rapid compared to the timescale for adiabatic heating and/or cooling (which is nearly always the case in our calculations), the sound speed of the gas is not determined by its true temperature, but rather by an effective sound speed that averages over the multi-phase ISM, turbulence, etc. The effective sound speed as a function of density can be interpolated freely between two extremes using a parameter q_{eos} . At one extreme, the gas has an effective sound speed of 10 km s^{-1} , motivated by, e.g., the observed turbulent velocity in atomic gas in nearby spirals; this is the “no-feedback” case with $q_{\text{eos}} = 0$. The opposite extreme, $q_{\text{eos}} = 1$, represents the “maximal feedback” sub-resolution model of Springel & Hernquist (2003), motivated by the multiphase ISM model of McKee & Ostriker (1977); in this case, 100% of the energy from supernovae is assumed to stir up the ISM. This equation of state is substantially stiffer, with effective sound speeds as high as $\sim 200 \text{ km s}^{-1}$. Varying q_{eos} between these two extremes amounts to varying the effective sound speed of the ISM, with the interpolation

$$c_s = \sqrt{q_{\text{eos}} c_s^2[q=1] + (1 - q_{\text{eos}}) c_s^2[q=0]}. \quad (4)$$

In addition to this effective equation of state, GADGET models star formation by stochastically converting gas particles into star particles at a rate determined by the gas density,

$$\dot{\rho}_{SF} = \frac{1 - \beta}{t_*^0 \rho_{th}^{1/2}} \rho^{1/2} \rho_c \propto \rho^{3/2} \quad (5)$$

where $\beta = 0.1$ is the fraction of the mass of a stellar population returned to the ISM by stellar evolution. The parameter t_* is the characteristic timescale for gas to be converted into stars at the threshold density $\rho_{th} = 0.092 \text{ cm}^{-3}$; $\rho_c \approx \rho$ is the density of the cold clouds, which is related to the density of the SPH particle by equations (17) and (18) of Springel & Hernquist (2003). For a given gas equation of state, the parameters in equation 5 can be adjusted to produce a global star formation law similar to the observed Kennicutt-Schmidt relations (Springel et al. 2005b).

For parameters in the equation of state model that have been used in previous work (Springel et al. 2005b) – $T_{SN} = 4 \times 10^8 \text{ K}$, $A_0 = 4000$, $t_*^0 = 8.4 \text{ Gyr}$ and $q_{EOS} = 0.5$ – we find that the model overpredicts the sound speed relative to the observed “turbulent” velocities of galaxies, i.e., the non-thermal line widths (see Fig. 1 of Hopkins & Quataert 2009 for a compilation of relevant data). For instance, the

Table 1. Simulation Parameters

Run Name	M_{tot} [M_{fid}] ^a	$f_{g,0}$	$\frac{M_b}{M_d}$	N_p [10^6]	ϵ [pc]	$\frac{R_{acc}}{\epsilon}$	α	τ	$M_{*,new}$ [$10^{10} M_\odot$]	$M_{BH,f}$ [$10^8 M_\odot$]	$M_{BH,p}$ [$10^8 M_\odot$]	σ_f [kms^{-1}]
fid	1.0	0.1	0.33	1.6	47	4	0.05	10	1.34	1.49	1.33	169
fidNof ^b	1.0	0.1	0.33	1.6	47	4	0.15	0	1.36	18.1	13.5	170
fid3a	1.0	0.1	0.33	1.6	47	4	0.15	10	1.34	1.03	0.90	168
fid6a	1.0	0.1	0.33	1.6	47	4	0.3	10	1.35	0.86	0.77	167
fidTau	1.0	0.1	0.33	1.6	47	4	0.05	3	1.36	5.05	4.31	163
fidt25	1.0	0.1	0.33	1.6	47	4	0.05	25	1.35	0.39	0.35	169
fid8eps	1.0	0.1	0.33	1.6	47	8	0.05	10	1.35	2.70	1.76	163
fidafg	1.0	0.1	0.33	1.6	47	4	* ^c	10	1.32	1.21	1.02	169
fidq2 ^d	1.0	0.1	0.33	1.6	47	4	0.05	10	1.30	1.40	1.16	168
fidq07 ^e	1.0	0.1	0.33	1.6	47	4	0.05	10	1.32	1.52	1.36	164
big	3.0	0.1	0.33	1.6	68	4	0.05	10	3.08	6.24	5.27	232
big6a	3.0	0.1	0.33	1.6	68	4	0.3	10	4.17	7.86	5.15	227
mid	0.3	0.1	0.33	1.6	32	4	0.05	10	0.39	0.38	0.26	115
small	0.1	0.1	0.33	1.6	22	4	0.05	10	0.13	0.24	0.13	82
small6a	0.1	0.1	0.33	1.6	22	4	0.3	10	0.13	0.25	0.24	84
smallq07 ^e	0.1	0.1	0.33	1.6	22	4	0.05	10	0.12	0.06	0.05	81
fg	1.0	0.3	0.33	2.4	47	4	0.05	10	4.41	7.10	5.53	159
smallfg	0.1	0.3	0.33	2.4	22	4	0.05	10	0.36	0.31	0.23	98
bulge	1.0	0.1	0.20	1.6	47	4	0.05	10	1.38	1.44	1.25	161
LRfid	1.0	0.1	0.33	0.16	102	4	0.05	10	1.34	1.65	0.93	164
MRfid	1.0	0.1	0.33	0.48	70	4	0.05	10	1.35	2.92	2.40	168
MRfidNof ^b	1.0	0.1	0.33	0.48	70	4	0.15	0	1.34	13.5	11.4	167
LRfidNof ^b	1.0	0.1	0.33	0.16	102	4	0.15	0	1.31	13.1	11.4	175
fidvol	1.0	0.1	0.33	1.6	47	8.62	0.05	10	1.39	3.22	2.45	164
MRfidvol	1.0	0.1	0.33	0.48	70	5.97	0.05	10	1.36	3.30	1.92	164

Columns are defined as follows: M_{tot} is the total mass in the simulation, $f_{g,0}$ is the initial gas fraction of the disk, M_b/M_d is the bulge to disk mass ratio, N_p is the total number of particles used in the simulation, ϵ is the Plummer equivalent gravitational force softening, R_{acc} , α and τ are the parameters of the BH accretion and feedback model (§2.3), $M_{*,new}$ is the total mass of new stars formed during the simulation, $M_{BH,f}$ and $M_{BH,p}$ are the masses of the BH at the end of the simulation and after the peak of accretion (defined to be when the accretion rate drops to one tenth its maximum value), respectively, and σ_f is the stellar velocity dispersion of the merger remnant (§4).

^a $M_{fid} = 3.88 \times 10^{12} M_\odot$.

^b These runs had no AGN feedback.

^c α was set by the gas fraction within R_{acc} using $\alpha = 3f_g^2$.

^d The ISM equation of state is defined using $q_{eos} = 0.2$ (see §2.2).

^e The ISM equation of state is defined using $q_{eos} = 0.07$ (see §2.2).

above model parameters imply $c_s \sim 30 \text{ km s}^{-1}$ at $n \sim 1 \text{ cm}^{-3}$ and $c_s \sim 110 \text{ km s}^{-1}$ at $n \sim 10^3 \text{ cm}^{-3}$. These values are too large by a factor of $\sim 2 - 3$ compared to the random velocities inferred from atomic and molecular line observations (Downes & Solomon 1998). To account for this, we set $q_{eos} = 0.5$ and then modified GADGET by reducing the pressure everywhere by a factor of 10. This reduces the effective sound speed by a factor of ~ 3 and is thus more consistent with observations. This reduction in ISM pressure is also used in the initial conditions when setting up vertical hydrostatic equilibrium for the gas. Changing the pressure requires changing the equation of state parameters to $T_{SN} = 6.6 \times 10^8 \text{ K}$, $A_0 = 6600$, and $t_*^0 = 13.86 \text{ Gyr}$ to maintain an average star formation rate of $1 M_\odot \text{ yr}^{-1}$ for an isolated galaxy with our fiducial Milky Way like mass. In §3.3 we compare our fiducial calculations with this reduction in pressure to models with smaller values of q_{eos} , 0.07 and 0.2; these also have smaller “sound speeds” more comparable to the observed random velocities of galaxies.

The reduction in the sound speed decreases the Jeans length and mass, making it numerically more prohibitive to resolve these critical scales. For the simulations presented here, we are careful to use sufficient numbers of particles so that the Jeans length and mass are always adequately resolved. The higher gas fraction simulations require a higher particle number as a result (see Table 1). The reduction in sound speed also makes it more likely that the gas will fragment by gravitational instability into clumps (ala molecular clouds), as we shall discuss in detail later. This fragmentation is real, not numerical; artificially increasing the sound speed to eliminate it is not necessarily physical and could give incorrect results. On the other hand, we do not include sufficient physics in our ISM model to describe the formation and disruption of molecular clouds so our treatment of the resulting clumping is also not correct. In §3.3 we discuss which of our results are the most sensitive to uncertainties related to local gravitational instability in the ISM.

2.3 Black Hole Accretion and Feedback

2.3.1 Black Hole Accretion Model

We include a BH as an additional collisionless particle at the center of each galaxy. We model the accretion of the surrounding gas onto the BH, via the transport of angular momentum, using

$$\dot{M}_{visc} = 3\pi\alpha\Sigma\frac{c_s^2}{\Omega} \quad (6)$$

where Σ is the mean gas surface density, Ω is the rotational angular frequency, and α is the dimensionless viscosity (a free parameter of our model). We compute Σ and c_s by taking an average of the properties of the SPH particles in a sphere of radius R_{acc} centred on the BH. The radius R_{acc} is typically set equal to four times the gravitational force softening length, i.e., $R_{acc} = 4\epsilon$, although we explore alternate choices as well. We find that estimating the rotation rate using $\Omega^2 \simeq GM(< R_{acc})/R_{acc}^3$ is more numerically robust than actually calculating the rotation and angular momentum of the gas particles within R_{acc} .

Although equation (6) is reminiscent of the alpha prescription of Shakura & Sunyaev (1973), in our formulation α characterizes not only the efficiency of angular momentum transport, but also the uncertainty due to the fraction of the inflowing gas that is turning into stars vs. being accreted onto the central BH. The physical mechanisms driving gas from $\sim \text{kpc}$ to $\sim 0.1 \text{ pc}$ are not fully understood, but non-axisymmetric gravitational torques are likely responsible (Shlosman et al. 1989; Hopkins & Quataert 2009). Using numerical simulations that focus on the nuclei of galaxies (from $\sim 0.1 - 100 \text{ pc}$) Hopkins & Quataert (2009) simulate the conditions under which there is significant gas inflow to $\lesssim 0.1 \text{ pc}$. They argue that the net accretion rate is not a strong function of the gas sound speed (unlike *both* eqns 1 and 6) because non-axisymmetric gravitational perturbations produce orbit crossing and strong shocks in the gas. The resulting inflow rate depends primarily on the non-axisymmetry in the potential, rather than the thermodynamics of the gas. Nonetheless, equation (6) evaluated at $\sim 100 \text{ pc}$ and with $\alpha \sim 0.1$ approximates the accretion rate at small radii in their simulations, albeit with substantial scatter (factor of ~ 10). Given that one of our key results discussed in §3 is that the accretion rate is not sensitive to the exact value of α , we believe that equation (6) is sufficient for the exploratory calculations in this paper.

2.3.2 Mass of the Black Hole Particle

In our galaxy merger simulations, the two BHs are initially far apart but approach each other in the late stages of the merger. When the BH particles have a separation of less than R_{acc} we consider them to have merged. When this occurs, we sum the individual masses of the two BH particles and set one of the particles to have this mass. This particle is then moved to the center of mass of the two BH system and given the velocity of the center of mass frame. The other BH particle is removed from the region.

The BH particles are subject to stochastic motion due to interaction with the stellar and gaseous particles, which leads to inaccuracy in the position of the BH and noise in the estimate of the accretion rate. To reduce this numerical “Brownian” motion, the BH particles are given a large

“tracer” mass of $2 \times 10^8 M_\odot$ for the fiducial simulation, and scaled with the overall mass for other simulations. As a result, the BH particle is a factor ~ 100 more massive than the halo particles, and a factor $\sim 10^4$ more massive than the stellar and gaseous particles. We artificially increase the BH particle mass solely to reduce numerical relaxation effects. This does not result in spurious dynamical effects on the central stars, gas, and dark matter since the BH’s sphere of gravitational influence extends to $\lesssim 10 \text{ pc}$ for the fiducial simulation, which is significantly smaller than our typical force softening of $\sim 50 \text{ pc}$.

For the results presented below, the “real” mass of the BH ($\equiv M_{BH}$) is computed by integrating the accretion rate of equation (6) in time. The gas particles are not removed as the BH mass increases. Instead, the gas particles have an additional label that tracks whether or not they have been “consumed.” We track how much mass the BH should have consumed via accretion at a given time, and the mass of gas that has been consumed. When there is a mis-match, we tag a number of gas particles within R_{acc} (chosen at random) as “consumed” until the total mass accreted by the BH is correct. Particles that have been consumed no longer contribute to the accretion rate estimate, even if they are inside R_{acc} . This implementation prevents any gas particle from providing more than its mass to the integrated mass of the BH.

2.3.3 Feedback from the Black Hole

In our simulations, the AGN is assumed to couple to the surrounding gas by depositing momentum into the gas, directed radially away from the BH. This crudely approximates the effects of (1) strong outflows and/or cosmic-ray pressure produced by the AGN (King 2003; Sironi & Socrates 2010) and (2) radiation pressure produced by the absorption and scattering of the AGN’s radiation by dust in the ISM (Murray et al. 2005). We focus on the latter when motivating the parameters used in our models.

To accurately account for the impact of the AGN’s radiation on gas in its host galaxy would require a radiative transport calculation, which is beyond the scope of the current work. Instead, we model this radiation pressure by depositing a total momentum per unit time of

$$\dot{p} = \tau \frac{L}{c} \quad \text{where } L = \min(\eta \dot{M}_{visc} c^2, L_{Edd}) \quad (7)$$

radially away from the BH into the SPH particles within a distance of R_{acc} of the BH particle. This momentum is equally distributed among the particles so that each particle experiences the same acceleration. We use a radiative efficiency of $\eta = 0.1$ in all simulations. The physical picture behind our feedback model in equation (7) is that the feedback is produced by the absorption of the ultraviolet light from the AGN by dust in the surrounding gas, and the subsequent reemission of infrared radiation that must diffuse its way out of the nuclear region. As described shortly, the parameter τ is the total infrared optical depth of the nuclear region.

To motivate equation (7) in more detail, we note that AGN radiate most of their radiation in the ultraviolet. The opacity of dusty gas to UV radiation is $\kappa_{UV} \sim 10^3 \text{ cm}^2 \text{ g}^{-1}$, so that only a surface density of $\sim 10^{-3} \text{ g cm}^{-2}$ is required

to absorb the UV radiation. This is far less than the typical radial column density of gas in the central $\sim 0.1 - 1$ kpc of luminous star forming galaxies, galaxy mergers, or our simulations (see Fig. 2 below). As a result, the UV radiation is efficiently absorbed, except perhaps along polar lines of sight. The absorption and scattering of the UV radiation deposits a momentum per unit time of L/c into the ambient gas, assuming for simplicity that all of the UV radiation is absorbed. If the infrared optical depth is $\gtrsim 1$, the infrared radiation re-emitted by the dusty gas must diffuse out through the nuclear region; doing so deposits an additional momentum per unit time of $\tau L/c$, where $\tau \sim \kappa_{IR}\Sigma$ is the infrared optical depth and $\kappa_{IR} \sim \text{few-}10 \text{ cm}^2 \text{ g}^{-1}$ is the infrared opacity for the radiation temperatures of interest $\sim 100 - 1000 \text{ K}$. The net force due to the UV and infrared radiation is thus $\dot{p} \sim (1 + \tau)L/c \simeq \tau L/c$, i.e. equation (7), for $\tau \gtrsim 1$, which is valid in our calculations near the peak of activity when the BH gains most of its mass.

In our calculations we use a constant value of τ rather than a time variable τ given by $\tau = \kappa_{IR}\Sigma$. Given the simplicity of our feedback model relative to a true radiative transfer calculation, this is not an unreasonable approximation. It is also easier to isolate the effects of varying τ when it is constant in time.

As noted above, we apply the force in equation (7) to all particles within a distance R_{acc} of the BH. A more accurate treatment would be to apply the force out to the point where the column is $\sim \kappa_{IR}^{-1}$, i.e., to where the optical depth to infinity is ~ 1 . At many times, however, this radius is unresolved. Moreover, it is possible that the photons diffuse primarily along the rotation axis of the gas, rather than in the orbital plane. As a result, the radiation pressure force will be applied primarily at small radii. This is why we apply the force only within R_{acc} . One consequence of this is that the number of SPH particles experiencing the feedback, N , will change as gas moves in and out of R_{acc} . Thus, the strength of feedback felt by an individual particle will change with time. However, because the SPH particles are collisional, they readily share this momentum with neighboring gas particles. In test problems described in Appendix B the effects of our feedback model are essentially independent of N and R_{acc} . The results are not quite so clean in our full simulations (see §3.2 and Appendix A), but nonetheless none of our major results depend sensitively on the region over which the feedback force is applied.

One might worry that if the number of particles within R_{acc} were too small, the momentum supplied to a single particle would become large enough to artificially accelerate the particle to the escape velocity. The minimum N required to avoid this is actually quite modest for the range of luminosities in our calculations, and for the simulations presented here this concern is never an issue (although it is for some of the test problems in Appendix B).

2.4 Parameter Choices for the Black Hole Model

Our model for BH growth and feedback contains three free parameters: (1) α determines the magnitude of the accretion rate onto the BH; (2) τ determines the total radiation pressure force produced by accretion onto the BH; it is roughly the optical depth to the far IR in the nuclear region; and (3) R_{acc} is the radius of the spherical region within which the accretion rate is determined and the feedback is applied. Our

fiducial values for these parameters are $\alpha = 0.05$, $\tau = 10$, and $R_{acc} = 4\epsilon$ (where ϵ is the gravitational force softening). We now motivate these particular choices.

The fiducial value of the viscosity used in this work is $\alpha = 0.05$, motivated by the rough consistency between the resulting \dot{M} and Hopkins & Quataert (2009)'s numerical simulations of gas inflow from $\sim 100 \text{ pc}$ to $\sim 0.1 \text{ pc}$ (although there is factor of ~ 10 scatter in the latter that is not captured here). Hopkins & Quataert (2009)'s calculations in fact require a more complicated subgrid accretion model that depends on additional parameters such as the bulge to disk ratio of the galaxy (because this influences the strength of non-axisymmetric torques); this will be explored in more detail in future work. In addition to $\alpha = 0.05$, we also carried out simulations with $\alpha = 0.15$ and $\alpha = 0.3$, and found no significant differences, for reasons explained below.

We use a constant value (with time) of $\tau = 10$ in most of our simulations. This is motivated by far infrared opacities of $\kappa_{IR} \sim 3 - 10 \text{ cm}^2 \text{ g}^{-1}$ and surface densities of $\Sigma \sim 1 - 10 \text{ g cm}^{-2}$ within R_{acc} during the peak of activity in our simulations. These surface densities are also consistent with those directly measured in the nuclei of ultra-luminous infrared galaxies (Downes & Solomon 1998). Given the uncertainties associated with the radiative transfer of far infrared photons in galactic nuclei, it is not possible to more accurately estimate the effective value of τ without detailed radiative transfer calculations. As we shall demonstrate explicitly, however, the exact value of τ is also not that critical for the qualitative effects of AGN feedback; the value of τ does, however, strongly affect the final value of the BH mass.

In choosing a value for R_{acc} , we must satisfy $R_{acc} > \epsilon$ in order to avoid numerical artifacts. In addition, we find that the BH particle remains within 4ϵ of the centre of mass of the system at nearly all times, but it can wander around within this region. As a result, 4ϵ is the smallest we can make R_{acc} without having noise induced by the BHs motion. This choice corresponds to several hundred pc in our typical simulation. Larger values of R_{acc} are unphysical because (1) the accretion rate should only depend on the gas close to the BH; i.e., the transport of gas from, for example, $\sim 8\epsilon$ to $\sim 2\epsilon$ is presumably adequately described by our simulations so we should not try to also account for this in our subgrid model, and (2) the radiation pressure force produced by the AGN (and the re-radiated infrared photons) is likely concentrated at relatively small radii, for the reasons described in §2.3.

3 GALAXY MERGER SIMULATIONS

Table 1 summarizes the simulations we focus on in this paper, including the resolution, the parameters that specify the initial conditions for the merging galaxies, the parameters that specify the BH accretion and feedback models, and the final properties of the merger remnants (stellar and BH mass and velocity dispersion). We begin by describing the results from our fiducial simulation (top row in Table 1) and then discuss simulations that vary a single parameter of the feedback model relative to the fiducial run. We have also performed simulations at different overall galactic mass scales, initial gas fractions, and numerical resolution. The latter resolution tests are presented in Appendix A.

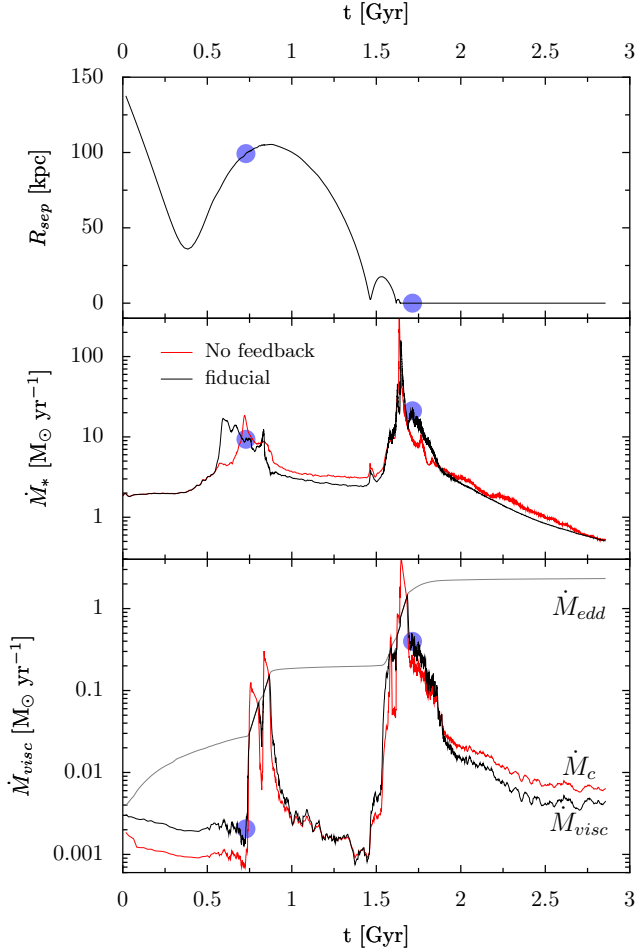


Figure 1. *Top:* The separation of the black hole particles as a function of time in the fiducial simulation. The blue circles label the times of the images shown in Figure 3. *Middle:* The star formation rate as a function of time for the fiducial simulation (black) and for the run with no feedback (red; run fidNof). *Bottom:* The viscous accretion rate, \dot{M}_{visc} (black), and Eddington rate (grey), as functions of time for the fiducial simulation. The critical \dot{M}_c at which radiation pressure balances gravity (eq. 8) is shown within a radius of R_{acc} (red; solid). The increase in star formation and BH accretion after first passage ($t \sim 0.75$ Gyr) is due to the fragmentation and inspiral of large gaseous/stellar clumps (Fig. 3), while the much larger increase at final coalescence is due to inflow of diffuse gas caused by non-axisymmetric torques. The latter physics dominates the total stellar and BH mass formed during the merger.

3.1 The Fiducial Simulation

The top panel of Fig. 1 shows the separation of the BH particles for the fiducial simulation, while the middle panel shows the total star formation rate (in both galaxies) for simulations with (black) and without (red) BH feedback. The first close passage of the two galaxies is around $t = 0.33$ Gyr and the system then undergoes a few short oscillations as the BHs finally settle into a merged state around $t = 1.65$ Gyr. The star formation rate increases following the first passage, with a much larger increase in the star formation rate during the final merger of the galaxies. The bottom panel of Fig. 1 shows the BH accretion rate determined from equation 6 (black) and the Eddington accretion rate (grey;

$\dot{M}_{edd} \equiv L_{edd}/(0.1c^2)$; the initial BH mass is $1.4 \times 10^5 M_\odot$ but as long as it is not too large $\gtrsim 10^8 M_\odot$, the precise initial BH mass is unimportant for our conclusions. In this and similar plots throughout the paper, the value of \dot{M} plotted before the BHs merge is for the BH in the galaxy with the smaller initial inclination relative to the orbital plane; the BH accretion rate for the other galaxy is comparable to that shown here. The evolution of the accretion rate is similar in many of the simulations we have carried out, with an initial period of activity after the first passage of the merging galaxies, and another period of even higher \dot{M} after the final coalescence of the galaxies and BHs. The latter active episode is when the merged BH gains most of its mass. In particular, the BH reaches the Eddington limit, allowing the mass of the BH to grow exponentially for a few hundred Myr.

DeBuhr et al. (2009) showed that the BH accretion and feedback model presented in this work leads to self-regulated BH growth, due to a competition between the (inward) gravitational force produced by the galaxy as a whole and the (outward) radiation pressure force produced by the central AGN (eq. 7) (Murray et al. 2005). For a spherically symmetric system, equating these two forces leads to $\tau L/c = 4f_g \sigma^4/G$, where $\sigma^2 = GM_t/2R_{acc}$, M_t is the total mass inside R_{acc} , and we have evaluated these expressions within R_{acc} , where our accretion rate is determined and feedback is implemented. Equivalently, there is a critical accretion rate \dot{M}_c , analogous to the Eddington rate, at which the two forces balance:

$$\dot{M}_c = \frac{4f_g}{\eta\tau Gc} \sigma^4. \quad (8)$$

The bottom panel of Fig. 1 shows \dot{M}_c for our fiducial simulation, evaluated within R_{acc} of the BH (solid red). Comparing \dot{M}_c to the BH accretion rate \dot{M}_{visc} demonstrates that during the peak episodes of accretion $\dot{M}_{visc} \sim \dot{M}_c$, so that radiation pressure becomes dynamically important. Although it is certainly possible to have accretion rates smaller than \dot{M}_c when there is insufficient gas to fuel the AGN, the accretion rate is limited to a maximum value of $\sim \dot{M}_c$.

Fig. 2 shows the surface density of gas within $R_{acc} = 4\epsilon = 0.19$ kpc for the fiducial simulation and for a higher gas fraction simulation with $f_g = 0.3$. As implied by Fig. 1, there are two main epochs during which significant gas is driven into the nuclei of the galaxies: after first passage and at final coalescence. The physical origin of these high nuclear gas densities are, however, somewhat different.

Mihos & Hernquist (1996) showed that the presence of a bulge like that in our simulation suppresses a nuclear starburst after first passage during galaxy mergers, because the bulge inhibits the non-axisymmetric modes that drive inflow. In our fiducial simulation, the majority of the increase in star formation after first passage is due to gravitational instability and fragmentation of the gas, which produces dense regions of rapid star formation. Fig. 3 (left panel) shows the gas density in the vicinity of one of the incoming black holes at $t = 0.74$ Gyr, midway through the first peak in star formation; the companion galaxy is well outside of this image. Two knots of dense gas are clearly seen, both of which will soon enter R_{acc} , the BH accretion and feedback region. These two clumps are not the only ones that form after first passage, but they are the only clumps that survive to enter

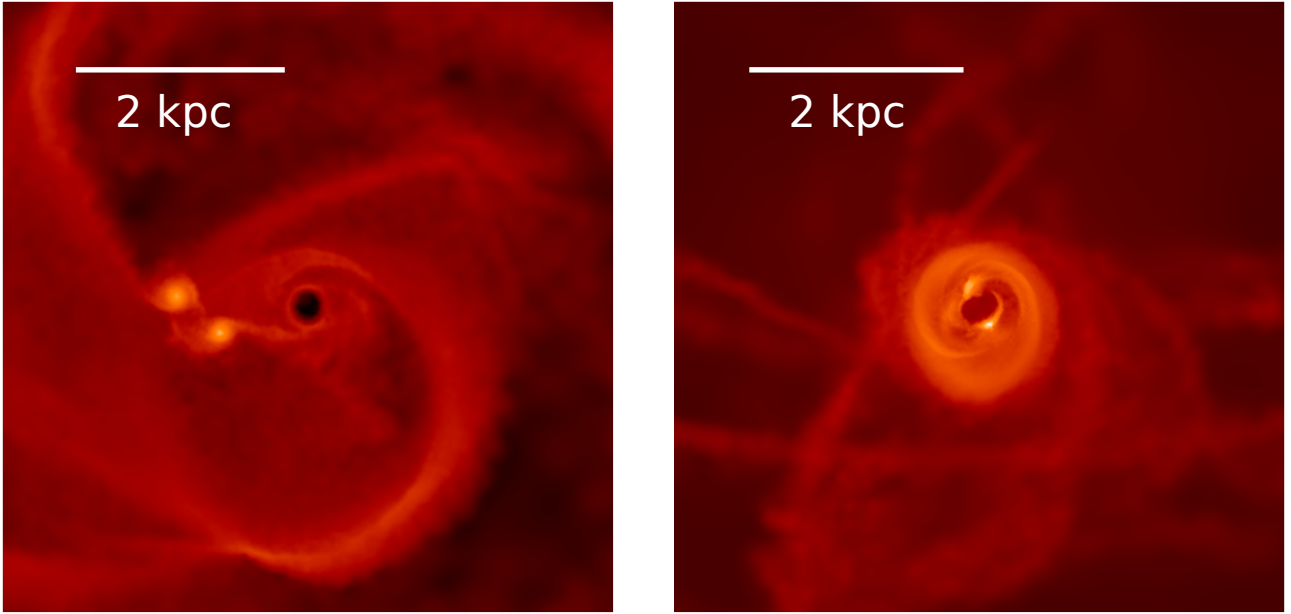


Figure 3. Gas density in the vicinity of the BH for the fiducial simulation at $t = 0.73$ Gyr (*left panel*), just prior to the onset of significant BH accretion after the first close passage of the two galaxies, and $t = 1.71$ Gyr (*right panel*), the peak of star formation and BH accretion after the galaxies and BHs have coalesced. The times of these images are labeled with blue circles in Figure 1. In the left panel, the image is for the less inclined galaxy and the companion galaxy is well outside the image. The images are 5.7 kpc on a side and brighter color indicates a higher density. The dark region in the center of each image is within R_{acc} of the BH and is evacuated by BH feedback. In the image just after first passage (*left panel*), the two bright white regions are gaseous/stellar clumps that fragmented by Toomre instability during first passage and then spiraled into the nucleus, fueling star formation and BH accretion. At final coalescence (*right panel*), the nuclear gas densities are significantly higher (see also Fig. 2) and most of the gas resides in a ~ 1 kpc diameter disk driven into the nucleus by non-axisymmetric stellar torques during the merger. These images were made using SPLASH (Price 2007).

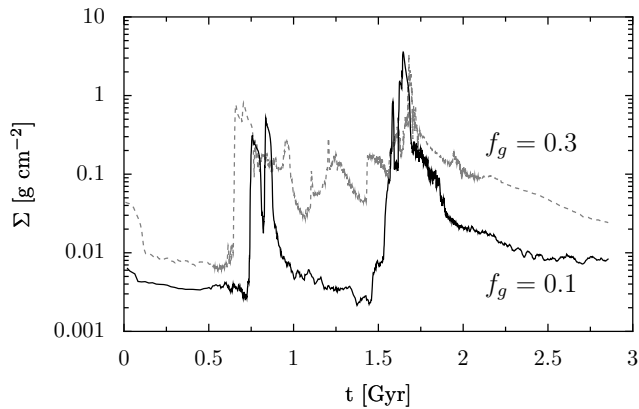


Figure 2. The mean gas surface density Σ interior to the accretion radius $R_{acc} = 4\epsilon = 0.19$ kpc for the fiducial simulation with initial gas fraction $f_g = 0.1$ (solid) and for the simulation with $f_g = 0.3$ (dashed; run fg).

the central region surrounding the BH.² Fig. 3 (right panel) also shows an image of the gas density in the nuclear region at $t = 1.71$ Gyr, near the peak of star formation and BH accretion and after the galaxies and BHs have coalesced. At this time, the gas density in the nuclear region is signifi-

² In the simulation with a higher initial gas density ($f_g = 0.3$), so many fragments form at large radii and spiral into R_{acc} that the surface density in the central region remains elevated from first passage until the merger completes at $t \sim 1.8$ Gyr (see Fig. 2).

cantly higher than at first passage (see also Fig. 2) and most of the gas resides in a ~ 1 kpc diameter disk. This nuclear gas concentration is the diffuse ISM driven in from larger radii by non-axisymmetric stellar torques during the merger (e.g., Mihos & Hernquist 1996).

The galaxies in our fiducial simulation are stable when evolved in isolation. The merger itself drives the gas to fragment by locally exceeding the Jeans/Toomre mass. In reality, the gas in such clumps might disperse after \sim a Myr because of stellar feedback not included in our calculations (Murray et al. 2010). This would probably not significantly change our estimate of the star formation rate since we are already normalized to the observed Kennicutt relation; however, such dispersal would lead to little inflow of gas associated with the inspiral of stellar clusters and thus would suppress the first peak in BH accretion (see Hopkins & Quataert 2009 for a more detailed discussion). In §3.3 we will return to these issues and show that the total stellar mass and BH mass formed during the merger are relatively insensitive to the details of our assumed ISM model.

Fig. 4 shows the surface density of gas in the fiducial simulation (top panel) and for the run without feedback (bottom panel) as a function of distance from the BH at four times: the initial condition ($t = 0$), shortly after the first close passage of the two galaxies ($t = 0.85$ Gyr), near the peak of accretion ($t = 1.71$ Gyr) and at the end of the simulation ($t = 2.85$ Gyr). Once $\dot{M} \sim \dot{M}_c$ at first passage ~ 0.85 Gyr, gas is driven out of the nuclear region by the AGN's radiation pressure. Since at the same time gravita-

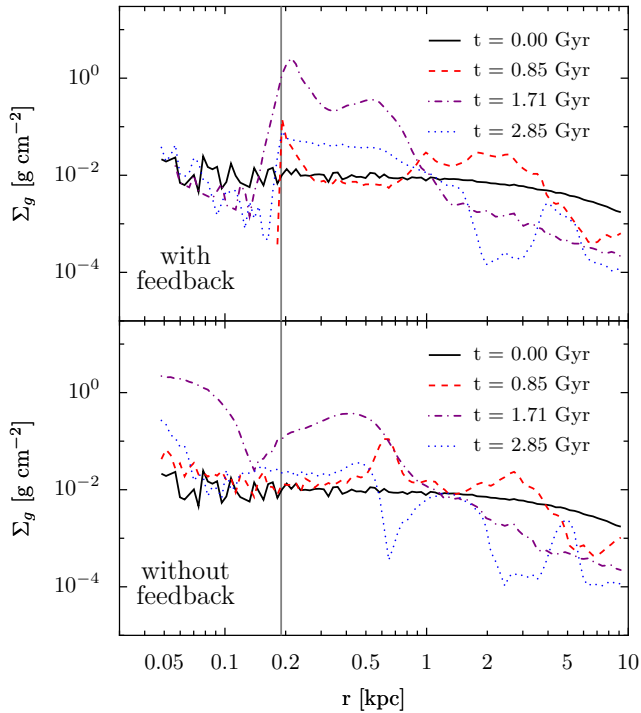


Figure 4. Comparison of gas surface density ($\equiv M_g[< r]/\pi r^2$) versus distance from the BH in the fiducial simulation with feedback (top) and without feedback (bottom). Four times are shown: $t = 0, 0.85$ Gyr (first passage), 1.71 Gyr (peak accretion), and 2.85 Gyr (end of simulation). Note that the gas tends to pile up at $R_{acc} = 0.190$ kpc (shown by the vertical line) in the top panel.

tional torques continue to drive gas inwards, the gas begins to pile up at $\sim R_{acc}$. The particular radius at which the pile up occurs of course depends on our choice of R_{acc} , and so the particular size of the evacuated region should not be taken too seriously. Qualitatively, however, the behavior in Fig. 4 is reasonable: the AGN pushes on the gas in its neighborhood until it deprives itself of fuel.

Near the peak of activity at $t = 1.71$ Gyr, the gas surface density in the central $R_{acc} \simeq 0.19$ kpc is a factor of $\sim 10 - 30$ larger in the simulations without feedback (bottom panel of Fig. 4). However, the gas density at large radii ~ 0.5 kpc is not that different. The radiation pressure force from the BH thus largely affects gas in its immediate environment, rather than the entire gas reservoir of the galaxy. Another indication of this is that the star formation rate is very similar in the simulations with and without feedback (middle panel of Fig. 1).

3.2 Dependence on Parameters of the BH Model

The models for BH accretion and feedback used here contain uncertain parameters. We have defined the three relevant parameters α , τ , and R_{acc} in §2.4 and motivated our fiducial values, but it is important to explore how our results change with variations about our fiducial parameters.

The value of α parameterizes the efficiency with which gas accretes from $\sim R_{acc} \sim 190$ pc to smaller radii, encapsulating both the efficiency of angular momentum transport and the effects of star formation on unresolved scales. Naively, a higher value of α would lead to a more mas-

sive BH. This is, however, not the case, because during the epochs when the BH gains most of its mass, the accretion rate is set by the efficiency of feedback (eq. 8) not by the available mass supply (see Figs 1 & 4). To demonstrate this more explicitly, the top left panel of Fig. 5 compares the BH accretion rates for three simulations with feedback, but differing values of α (0.05, 0.15, and 0.3), to the simulation with no feedback, which has $\alpha = 0.15$. The accretion histories for the three values of α are nearly identical. By contrast, the accretion rate is in general much larger in simulations that neglect feedback (and is $\propto \alpha$). In addition to the constant α runs, we tested a model in which α was time variable, set by the local gas fraction near the BH (fidafg2 in Table 1): $\alpha = 3f_g^2$, with f_g determined within R_{acc} (in practice α varied from $\sim 2 \times 10^{-4} - 0.3$). Although this precise functional form is somewhat arbitrary, such a variation is motivated by analytic arguments and numerical simulations which show that instabilities due to self-gravity dominate the transport of gas from ~ 100 pc inward (Shlosman et al. 1990; Hopkins & Quataert 2009). For our $\alpha = 3f_g^2$ simulation, we find that the peak accretion rates and final BH mass are very similar to the constant α simulations. This is consistent with our conclusion that in the limit of large fuel supply, feedback, rather than the efficiency of angular momentum transport, sets the rate at which the BH grows.

The parameter τ describes the efficacy of the feedback for a given AGN luminosity. The bottom left panel of Fig. 5 compares the BH accretion rate for the fiducial run with $\tau = 10$ (black) and a simulation with a smaller value of $\tau = 3$ (orange). To the extent that the accretion rate is feedback limited and set by \dot{M}_c in equation 8, \dot{M} should decrease with increasing τ . Physically, this is because larger τ leads to a larger feedback force, which then requires a smaller accretion rate to provide the luminosity necessary to drive away the surrounding gas. This expectation is borne out by the simulations. To compare the numerical results with the scaling in equation 8, the bottom left panel of Fig. 5 also shows \dot{M} for the fiducial simulation scaled by a factor of $10/3$ (dashed line). This scaled \dot{M} of the fiducial simulation is in reasonably good agreement with the $\tau = 3$ simulation, particularly at the first and second peaks in \dot{M} , when most of the BH's mass is accumulated. This demonstrates that the value of τ does not significantly affect any of the qualitative behavior of how the BH grows, although it does determine the overall value of the BH mass.

In the majority of the simulations presented here, the size of the region over which we apply the feedback and average the gas properties to calculate \dot{M} , R_{acc} , is set to 4ϵ . The rationale for this choice was given in §2.4, but it is important to consider the effects of changing this value. The top right panel of Fig. 5 shows the mass accretion rate for the fiducial simulation and a simulation with $R_{acc} = 8\epsilon = 380$ pc. The peak values of \dot{M} and the time of the first and second peaks are reasonably similar in the two cases. The principle difference is that in the simulations with the larger value of R_{acc} , the feedback is less effective at clearing gas out of the nuclear region (because the force is distributed over a larger number of particles); this allows a higher level of \dot{M} to be maintained after the first passage and final coalescence. We suspect that the fiducial simulation better approximates what a higher resolution calculation with radiative transfer would find, but this remains to be demonstrated.

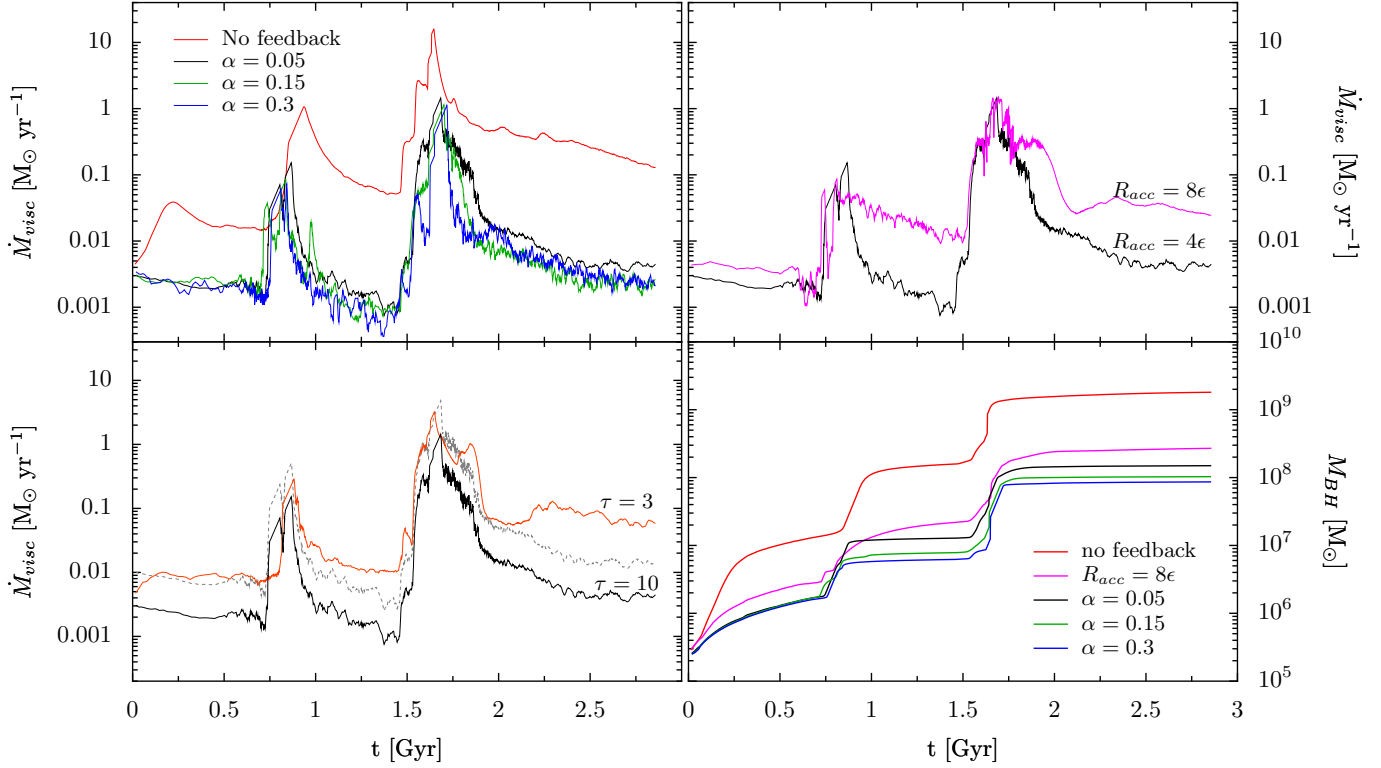


Figure 5. *Top Left:* Comparison of the accretion rates for the run without feedback (red; fidNof, $\alpha = 0.15$), and three runs with feedback: the fiducial simulation with $\alpha = 0.05$ (black), the run with $\alpha = 0.15$ (green; fid3a) and the run with $\alpha = 0.3$ (blue; fid6a). *Top Right:* The accretion rate for the fiducial run (black) and the run with $R_{acc} = 8\epsilon$ (magenta; fid8eps). *Bottom Left:* The accretion rate for the fiducial run (black) and the run with $\tau = 3$ (orange; fidTau). Also shown is \dot{M}_{visc} for the fiducial run increased by a factor of 10/3 (dashed line), as expected from eq. (8). *Bottom Right:* The integrated black hole masses for all the runs in this Figure with $\tau = 10$.

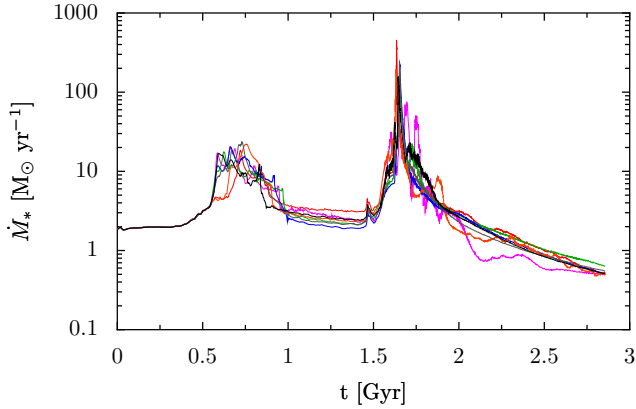


Figure 6. The star formation rate for the run with no feedback (red) and for runs with various values of the BH accretion and feedback parameters: $\alpha = 0.05, 0.15, 0.3$ (black, green, blue), $\alpha = 3f_g^2$ (grey), $\tau = 3$ (orange), and $R_{acc} = 8\epsilon$ (magenta). All of these models have very similar star formation histories.

The bottom right panel of Fig. 5 shows the integrated BH mass as a function of time for the fiducial simulation and for the variations in the feedback/accretion model considered in this subsection that have the same value of τ (but different values of α and/or R_{acc}). The key result is that in the presence of feedback (all but the top curve), there is only a factor of $\simeq 3$ change in the BH mass due to differ-

ences in how we treat BH accretion and feedback. A factor of 6 change in α leads to only a 42% change in the final BH mass. This is because most of the BH mass is gained during the final coalescence of the two galaxies, at which point the BH accretion self-regulates and reaches the Eddington-like value in equation (8). The run without feedback (top curve), by contrast, has a factor of ~ 10 larger BH mass and the BH mass would scale linearly with the assumed value of α .

The star formation rates for the simulations with different BH feedback parameters are all shown in Fig. 6 (this includes the fiducial simulation with and without feedback and the runs with $\alpha = 0.15, 0.3, 3f_g^2$, $\tau = 3$, and $R_{acc} = 8\epsilon$). This figure demonstrates that the precise parameters of the BH feedback model have little effect on the galaxy-wide properties such as the star formation rate: the total mass of stars formed in simulations with different BH feedback parameters differ by less than 5%.

In previous simulations of BH growth and feedback, AGN feedback acting on dense gas in galaxies has been invoked to quench star formation (Springel et al. 2005a). Our results demonstrate, however, that this is by no means guaranteed (we refer here to ‘quasar’ feedback on cold dense gas, not the effect of AGN on hot dilute gas in galaxy groups and clusters). In our calculations BH growth is self-regulated and closely connected to the properties of the surrounding galaxy (e.g., eq. 8). However, the BHs dynamical influence is centered in the galactic nucleus ($\lesssim 300$ pc); as a result, the BH does not significantly alter the star formation history during

a merger. In this scenario, the merger remnant can nonetheless be relatively quiescent (“red and dead”) because the burst of star formation uses up much of the available gas.

3.3 Effects of the ISM Model

Motivated by observations (e.g., Downes & Solomon 1998), we have reduced the effective sound speed in GADGET’s subgrid ISM model (see §2.2). There is nonetheless considerable uncertainty in the accuracy of this (or any other) subgrid model. To study in more detail the effects of the ISM model on our results, we performed two additional simulations at our fiducial galaxy mass with the subgrid interpolation parameter $q_{\text{eos}} = 0.2$ and 0.07 (see eq. 4), and without the factor of 10 reduction in pressure used in our fiducial simulation (an additional simulation with $q_{\text{eos}} = 0.07$ at a lower galaxy mass will be discussed in §4).³ The three different ISM models have c_s and Q within a factor of ~ 2 of one another at all radii, with the $q_{\text{eos}} = 0.2$ model having the largest values of c_s and Q , and our fiducial model having the smallest values. The parameter Q is initially ~ 3 for our fiducial simulation at the disk scale length R_d , which is why the merger can induce significant fragmentation of the gas (Fig. 3). Given the limited physics included in the subgrid model, we do not believe that it is feasible to unambiguously conclude which of these ISM models is more realistic. These models thus provide an indication of the systematic uncertainty introduced by our treatment of the ISM.

Fig. 7 compares the BH accretion history (top panel), the star formation rate (middle), and the integrated BH mass and mass of new stars formed during the merger (bottom) for the three runs with differing ISM models. For both the fiducial run and the run with $q_{\text{EOS}} = 0.07$ there is significant fragmentation after first passage, which generates the first peak in star formation and BH accretion. By contrast, the run with $q_{\text{EOS}} = 0.2$ shows no evidence for gas fragmentation or a pronounced peak in activity at first passage. Despite these differing initial histories, the final result of the merger is very similar in all three cases: the large star formation rates and BH accretion rates coincident with the final coalescence of the two galaxies are not due to fragmentation, but are instead largely due to the inflow of diffuse gas to smaller radii. Moreover, the final BH mass and the total amount of new stars formed during the merger are similar in all three cases. Thus, despite uncertainties in the model of the ISM, we find relatively robust integrated quantities (as did the earlier calculations of Hernquist & Mihos 1995). The precise time dependence of the star formation and BH accretion (i.e., the lightcurves) are, however, significantly more uncertain and sensitive to the details of the model.

3.4 Galaxy Parameters

Having shown that the final BH mass and new stellar mass do not depend strongly on the uncertain parameters in our accretion, feedback and ISM models, we now examine how our results vary with galaxy properties such as the total mass, gas fraction, and bulge-to-disk ratio.

³ We used $T_{\text{SN}} = 4 \times 10^8$ K, $A_0 = 4000$ and $t_*^0 = 8.4$ Gyr for these calculations; these values are different from those in our fiducial simulation, and are chosen to fix the total star formation rate for our isolated fiducial galaxy at $1 M_\odot \text{ yr}^{-1}$.

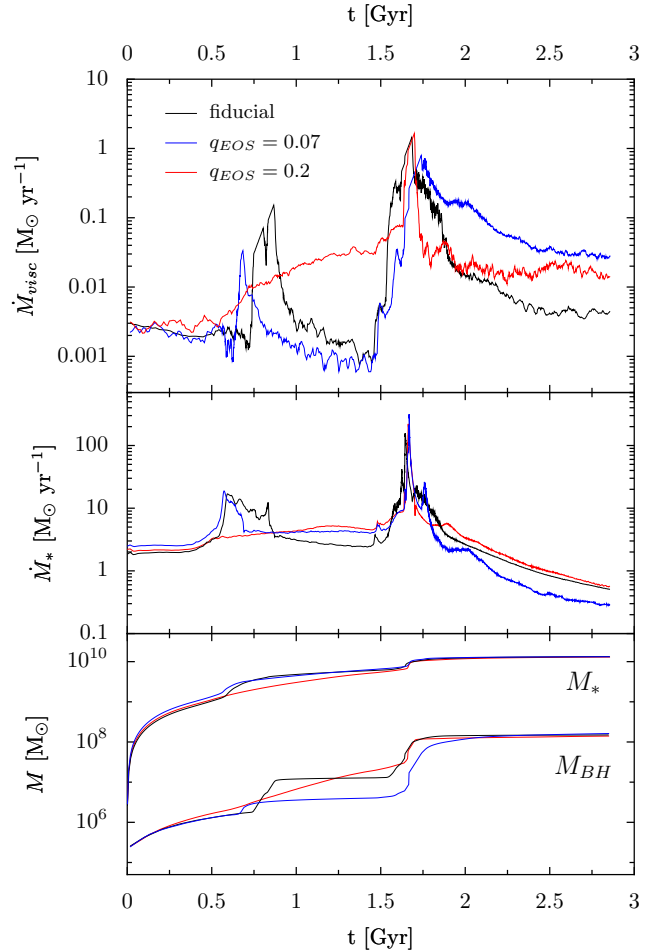


Figure 7. Comparison of three simulations that differ only in the ISM models: fiducial (black), $q_{\text{EOS}} = 0.2$ (red), and $q_{\text{EOS}} = 0.07$ (blue). The panels show the viscous accretion rate (top), star formation rate (middle), and the integrated black hole mass and mass of new stars formed (bottom). The three different ISM models have c_s and Toomre Q within a factor of ~ 2 of one another at all radii; the $q_{\text{eos}} = 0.2$ model has the largest values of c_s and Q and our fiducial model has the smallest values.

Fig. 8 shows the BH accretion histories (top panel), star formation rate (middle), and integrated BH mass (bottom) for four runs with different total galaxy mass. The models cover a factor of 30 in galaxy mass, from 0.1-3 times our fiducial mass. The BH and star formation parameters are identical in the four simulations, while the gravitational force softening and structural parameters (e.g., disk scale length, bulge radius) change with the total mass (see §2.1).

Fig. 8 shows that the BH accretion rates and integrated BH masses increase with galaxy mass as expected from equation 8. However, there is a clear difference between the lower and higher mass simulations: the two higher mass simulations show evidence for the first peak in star formation and BH growth that we have shown is due to fragmentation near first passage, while the lower mass runs do not. This is largely a consequence of the fact that observed disks have $R_d \propto M^{1/3}$ (Shen et al. 2003), so that more massive galaxies have higher surface densities and are thus more susceptible to gravitational instability (our ISM model counteracts

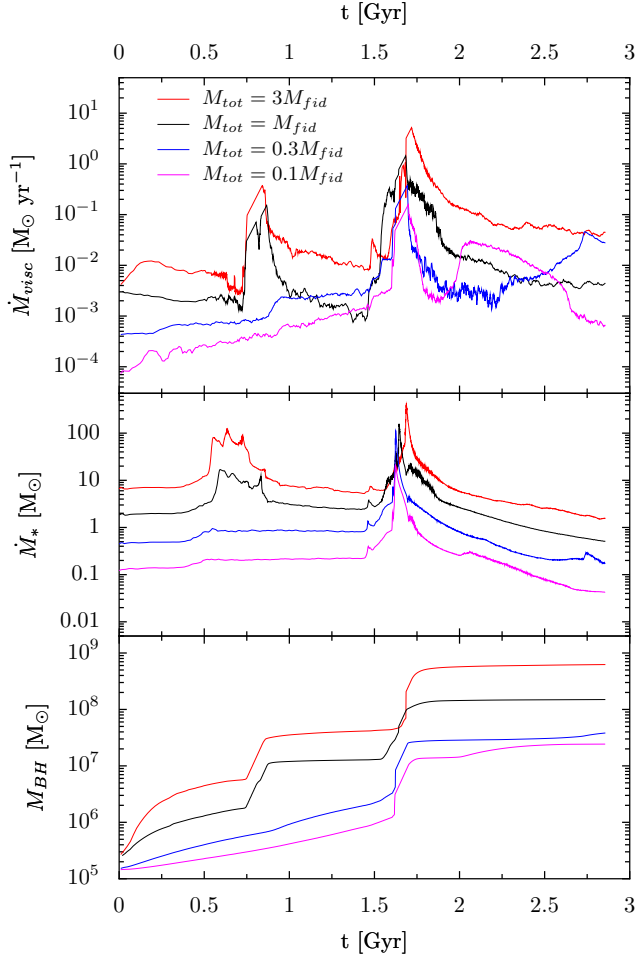


Figure 8. Comparison of four simulations that differ only in the total galaxy mass: $M_{fid} = 3.88 \times 10^{12} M_{\odot}$ (fiducial; black), $3M_{fid}$ (red), $0.3M_{fid}$ (blue), and $0.1M_{fid}$ (magenta). The three panels show the viscous accretion rate (top), star formation rate (middle), and the integrated black hole mass (bottom). The same parameters are used in the BH accretion and feedback models.

this slightly, but not enough to stabilize the higher mass disks). It is important to reiterate, however, that modest changes to the subgrid sound speed can change whether or not the gas fragments near first passage (§3.3) so it is not clear if the difference as a function of mass in Fig. 8 is robust.

In addition to the systematic change in the importance of fragmentation near first passage, Fig. 8 also shows differences in the late-time BH accretion between the low and high mass simulations. In particular the two smaller mass runs each show a period of increased accretion after the main peak during the merger. In these cases the new stars formed around final coalescence develop a bar in the inner $\sim R_{acc}$ of the galaxy. This helps drive some of the remaining gas into the accretion region leading to the increased accretion at late times. There is a milder version of this late-time accretion in the fiducial mass $q_{eos} = 0.2$ model without fragmentation in Fig. 7. Interestingly, there is no analogous late-time inflow of gas to within R_{acc} in our low mass galaxy simulations without BH feedback. The late-time activity is also particularly sensitive to the accretion model at a time when the non-axisymmetry produced by the merger has died

away (so that α may in reality decrease significantly). For these reasons, we regard the late time growth in Fig. 8 as an interesting deviation from self-similarity in the dynamics, but not necessarily a particularly robust one. One important point that this highlights, however, is that because our implementation of BH growth and feedback does not unbind a significant amount of cold gas at late times (unlike calculations by Springel et al. 2005a), the predictions of our model are more sensitive to the post galaxy coalescence physics.

In addition to the fiducial gas fraction ($f_g = 0.1$) simulations that we have largely focused on, we performed simulations with an initial gas fraction of $f_g = 0.3$ for our fiducial galaxy mass and at one tenth this mass. The qualitative difference in behavior with galaxy mass in Fig. 8 persists in the higher gas fraction runs. In particular, in the low mass $f_g = 0.3$ simulation, the gas does not fragment, while it does in the higher mass $f_g = 0.3$ simulation. Fig. 2 – discussed in §3.1 – explicitly shows the increase in the gas surface density within R_{acc} produced by this at early times.

A final property of the galaxy model that we varied was the bulge to disk mass ratio. The majority of our runs include a bulge with one third the mass of the disk; we also ran one simulation with an initial bulge of one fifth the disk mass, at the fiducial galaxy mass. The final BH mass and total mass of stars formed differ by less than 3% each compared to the fiducial simulation.

4 THE $M_{BH} - \sigma$ CORRELATION

Previous numerical studies using models of BH growth and feedback different from those considered here have reproduced a number of the observed correlations between massive BHs and their host galaxies (e.g., Di Matteo et al. 2005; Sazonov et al. 2005; Younger et al. 2008). Younger et al. (2008) argue that the galaxy-BH correlations in simulations (in particular, the BH fundamental plane) are relatively independent of the trigger of BH growth, be it minor mergers, major mergers, or global instabilities of galactic disks. Based on the calculations to date, however, it is unclear to what extent the simulated BH-galaxy correlations depend on the details of the BH feedback or accretion models. In this section we assess this question by quantifying the $M_{BH} - \sigma$ relation produced in our models.

We define σ of our model galaxies using a method analogous to that of observers: we first project the mass density of the stellar particles into cylindrical bins, and compute the half-mass(light) radius R_e . We then compute the velocity dispersion weighted by the surface brightness via

$$\sigma^2 = \frac{\int_{R_{min}}^{R_e} \sigma_{los}^2(R) I(R) R dR}{\int_{R_{min}}^{R_e} I(R) R dR} \quad (9)$$

where $I(R)$ is the projected 2-d stellar mass profile, σ_{los} is the line of sight velocity dispersion, and $R_{min} = 2\epsilon$ to ensure that there are that no artificial effects introduced by the force softening. We repeat this calculation along 1000 lines of sight with random viewing angles through the center of mass of the merger remnant. The σ quoted in this paper and listed in Table 1 is the median value over the 1000 lines of sight.

Fig. 9 shows the correlation between the final BH mass $M_{BH,f}$ and the σ of the merged galaxy for most of the simulations in Table 1: different total galaxy masses (black), dif-

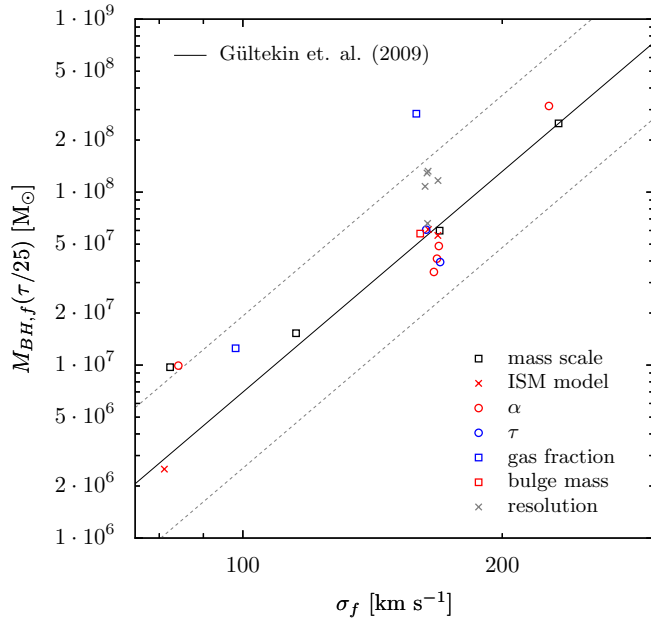


Figure 9. The $M_{BH,f}-\sigma$ relation for the simulations in this paper, along with the observed relation (solid) and one sigma scatter (dotted) from Gültekin et al. (2009). The final BH mass $M_{BH,f}$ in all of the simulations has been linearly scaled to $\tau = 25$ from the value used in the simulation (typically $\tau = 10$). The simulations are generally quite consistent with observations; we do find indications of a slight flattening in $M_{BH,f}-\sigma$ at low BH masses.

ferent values of the accretion parameter α (red circle), alternate ISM models (red x), higher gas fraction (blue square), alternate bulge mass (red square), different values of τ (blue circle), and the resolution studies in Appendix A (grey). The solid line indicates the mean relation from the compilation of observational results in Gültekin et al. (2009) while the dotted lines are the $1-\sigma$ error bars. We have linearly rescaled all of our final BH masses to a value of $\tau = 25$, using the fact that both the analytic and numerical results are consistent with \dot{M}_{visc} and $M_{BH,f}$ being $\propto \tau^{-1}$. The value of $\tau = 25$ is chosen so that the rescaled fiducial simulation lies approximately on the $M_{BH}-\sigma$ relation of Gültekin et al. (2009). For our fiducial simulation carried out with $\tau = 3$ and $\tau = 10$, a linear scaling of $M_{BH,f}$ with τ^{-1} is accurate to about 2% (e.g., Table 1 and Fig. 5). We also carried out our fiducial simulation with $\tau = 25$; this is consistent with a linear scaling of $M_{BH,f}$ from $\tau = 3$ to $\sim 50\%$ (Table 1). For nearly all of our simulations, rescaling to $\tau = 25$ amounts to dividing the final BH mass by a factor of 2.5.

Previous analytic arguments were able to reproduce the $M_{BH}-\sigma$ relation with $\tau \sim 1$, rather than requiring $\tau \sim 25$ as we do here (e.g., King 2003; Murray et al. 2005). These calculations, however, assumed $f_g = 0.1$. While perhaps appropriate on average, this is not appropriate in galactic nuclei where the gas densities are higher. The analytic derivations also assumed that BH growth terminated when the system reached the luminosity (accretion rate) at which radiation pressure balances gravity (eq. 8). In reality, however, the luminosity must exceed this critical value by a factor of several in order for gas to be efficiently pushed around in the galactic nucleus (as shown explicitly in the test problems in the Appendix). Moreover, the BH continues to accrete some

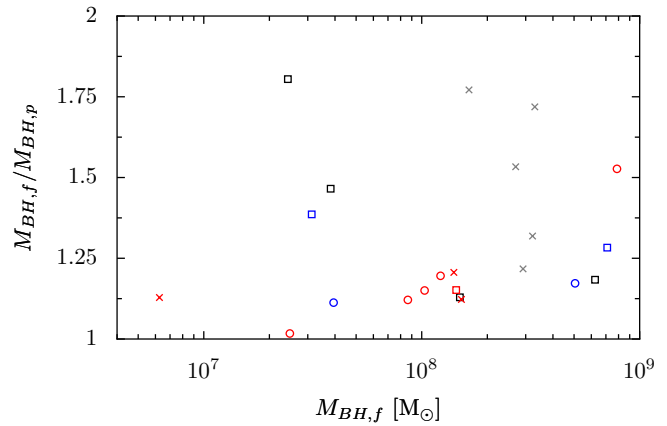


Figure 10. The ratio of the final BH mass to the BH mass at the peak of accretion for the simulations in Fig. 9, using the same symbol types. This quantifies the extent to which late-time accretion increases the BH mass. The late-time increase in BH mass for many of the lower mass systems produces the slight flattening in $M_{BH}-\sigma$ in Fig. 9 at low masses; see the text for a discussion of the robustness of this result.

mass even after reaching \dot{M}_c . Fig. 10 shows this explicitly via the ratio of the final BH mass to the BH mass at the peak of activity for all of the simulations in Fig. 9.⁴ The net effect of the differences between our simulations and the simple analytic calculations is that a much larger feedback force per unit BH mass ($\tau \sim 25$, not ~ 1) is required for consistency with the observed $M_{BH}-\sigma$ relation. The physical implications of this larger value of τ for models of AGN feedback will be discussed in § 5.

The scatter in BH mass in Fig. 9 at our fiducial mass scale of $\sigma \sim 175 \text{ km s}^{-1}$ is reasonably consistent with the observed scatter. In the simulations we have varied the BH accretion model (α), the ISM model, numerical resolution, size of the feedback/accretion region R_{acc} , and galaxy properties such as the total mass, gas fraction, and bulge to disk ratio. It is encouraging that all of these simulations produce BH masses within a factor of few of each other. The largest BH mass at $\sigma \sim 175 \text{ km s}^{-1}$ is the simulation with an initial gas fraction of $f_g = 0.3$; since this run has a larger gas density at small radii close to the BH (Fig. 2), it should probably also have a larger τ , which would reduce the BH mass further, in better agreement with the data. It is difficult to make this comparison to the observed scatter more quantitative given the limitation that our simulations are all equal-mass non-cosmological binary mergers on the same orbit.

The numerical results in Fig. 9 suggest a slight flattening of the $M_{BH}-\sigma$ relation at $\sigma \lesssim 100 \text{ km s}^{-1}$. This is in large part a consequence of the additional mass gained by the lower mass BHs after their peak of activity (see Figs. 8 & 10, in particular the fiducial simulations labeled by black squares in Fig. 10). This change in behavior at lower masses is primarily due to the fact that the lower mass galaxies are less prone to fragmentation than the more massive galaxies (§3.4). Without the fragmentation after first passage, more

⁴ To account for the fluctuating nature of the BH accretion rate in some of the simulations, we define the BH mass at “peak” to be the mass when \dot{M} drops by a factor of 10 from its peak value.

gas is available to feed the BH at late times leading to the slightly higher BH mass. As discussed in §3.4, it is unclear how robust this late time accretion is. In fact, a low mass galaxy simulation with an alternate ISM model ($q_{\text{eos}} = 0.07$) does not show significant late-time accretion, leading to a BH mass in good agreement with the extrapolation from higher σ (red x at low mass in Figs. 9 & 10). We thus regard the case for flattening of $M_{\text{BH}} - \sigma$ at low masses in our models as somewhat tentative; our results may instead indicate enhanced scatter at low masses rather than a change in the mean relation. More comprehensive numerical studies of these lower mass systems will be needed to distinguish these two possibilities.

5 DISCUSSION AND CONCLUSIONS

We have presented a new method for simulating the growth of massive BHs in galaxies and the impact of AGN activity on gas in its host galaxy (see also our related Letter; DeBuhr et al. 2009). In this method, we use a local viscous estimate to determine the accretion rate onto a BH given conditions in the surrounding galaxy (eq. 6), and we model the effect of BH feedback on ambient gas by depositing momentum radially away from the BH into the surrounding gas (eq. 7).

Our accretion model qualitatively takes into account the angular momentum redistribution required for accretion of cold gas in galaxies and is thus more appropriate than the spherical accretion estimate that has been used extensively in the literature. In our feedback model, the applied force is given by $\tau L/c$, where the AGN's luminosity L is determined by our BH accretion model, and the net efficiency of the feedback is determined by the total optical depth τ of the galactic gas to the AGN's radiation, which is a free parameter of our model. Previous calculations have demonstrated that only when the gas fraction in a galaxy decreases to $\lesssim 0.01$ can the AGN's radiation Compton heat matter to high temperatures (Sazonov et al. 2005). More generally, the cooling times in gas-rich galaxies are so short that the primary dynamical impact of the AGN on surrounding gas is via the momentum imparted by the AGN's outflows or radiation. It is thus not physically well-motivated to model AGN feedback by depositing energy, but not momentum, into surrounding gas, as many calculations have done (e.g., Di Matteo et al. 2005; Springel et al. 2005a; Kawata & Gibson 2005); see Ostriker et al. (2010) for related points.

Throughout this paper, we have focused on BH growth during major mergers of spiral galaxies. As demonstrated in DeBuhr et al. (2009), our model leads to a self-regulated mode of BH accretion in which the BH accretion rate is relatively independent of the details of the BH accretion model (see Fig. 5). This is because the accretion rate self-adjusts so that the radiation pressure force is comparable to the inward gravitational force produced by the host galaxy (see eq. 8). This self-regulated mode of BH accretion is a robust feature of all of our simulations during periods of time when there is a significant nuclear gas reservoir – it thus applies precisely when the BH gains most of its mass.

One important consequence of this self-regulated accretion is that AGN feedback does not drive significant large-scale outflows of gas (in contrast to the models of

Springel et al. 2005a). For example, the surface density profiles in Fig. 4 show that AGN feedback causes gas to pile up at a few hundred pc rather than being completely unbound from the galaxy – this precise radius should not be taken too literally since it is a direct consequence of the fact that we implement feedback and determine the BH accretion rate only within a radius $R_{\text{acc}} \sim$ few hundred pc. Nonetheless, we believe that this general result may well be generic: because the BH accretion rate is determined by the gas content close to the BH, the AGN can shut off its own accretion before depositing sufficient energy to unbind all of the gas in the galaxy. If we artificially hold the luminosity of the AGN constant in time at a value exceeding the critical value in equation (8), then the AGN *does* eventually unbind all of the surrounding gas (see, e.g., Figs. B1 & B3 in Appendix B). However, both our isothermal sphere test problem (Fig. B6) and our full merger calculations show that when the BH accretion rate is self-consistently determined by the gas properties in the central ~ 100 pc of the galaxy, the AGN simply never stays ‘on’ long enough to unbind all the gas.

Our results do not, of course, preclude that AGN drive galactic winds. For example, some gas may be unbound by a high speed wind/jet produced by the central accretion disk (which is not in our simulations). In addition, at later stages of a merger or at large radii the gas fraction can be sufficiently low ($\lesssim 0.01$) that gas can be Compton heated to high temperatures and potentially unbound (e.g., Ciotti et al. 2010). This may in fact be sufficient to quench star formation at late times, but only once most of the gas has already been consumed into stars (so that $f_g \lesssim 0.01$). Our results do suggest that AGN feedback does not quench star formation by unbinding a significant fraction of the cold dense gas in a galaxies interstellar medium (in contrast to, e.g., Springel et al. 2005a). In future work it will be important to assess whether variability in the accretion rate on smaller scales than we can resolve (e.g., Hopkins & Quataert 2009; Levine et al. 2010) modifies this conclusion; such variability could produce some epochs during which AGN feedback has a significantly larger effect on the surrounding gas. Another improvement would be to carry out radiative transfer calculations and assess what fraction of the AGN's radiation is absorbed at large radii in a galaxy (\sim kpc) where the gas has a lower surface density and is thus easier to unbind.

Our simulations cover a factor of ~ 30 in galaxy mass. The final BH mass in our calculations is $\propto \tau^{-1}$ since a larger value of τ corresponds to a larger momentum deposition per unit BH mass. We find reasonable consistency with the normalization of the observed $M_{\text{BH}} - \sigma$ relation for $\tau \sim 25$. To compare this result to previous work by Di Matteo et al. (2005), we note that a momentum deposition of \dot{P} corresponds to an energy deposition rate of $\dot{E} \simeq \dot{P}\sigma$ when the feedback is able to move the gas at a speed comparable to the velocity dispersion σ (which is required for efficient self-regulation of the BH growth). For $\tau \simeq 25$, our results thus correspond to $\dot{E} \simeq 25 L \sigma/c \simeq 0.02 L (\sigma/200 \text{ km s}^{-1})$. This is similar to the results of Di Matteo et al. (2005), who found that depositing $\sim 5\%$ of the BH accretion energy in the surrounding gas was required to explain the $M_{\text{BH}} - \sigma$ relation. It is encouraging that these two different sets of simulations, with different BH accretion and feedback models, agree at the factor of $\sim 2 - 3$ level on the energetics required to reproduce the $M_{\text{BH}} - \sigma$ relation.

The value of $\tau \sim 25$ required to explain the normalization of the $M_{BH} - \sigma$ relation has strong implications for the dominant physics regulating BH growth. The simplest models of super-Eddington winds from an accretion disk close to the BH are ruled out because they typically have $\tau \sim 1$, i.e., a momentum flux comparable to that of the initial radiation field (King 2003). Similarly, the radiation pressure force produced solely by the scattering and absorption of the AGN's UV radiation by dust corresponds to $\tau \sim 1$ (Murray et al. 2005) and is thus not sufficient to account for the level of feedback required here. Rather, our results suggest that most BH growth happens when the nuclear regions are optically thick to the re-radiated dust emission in the near and far-infrared, so that $\tau \gg 1$. This is consistent with observational evidence in favor of a connection between BH growth, quasars and luminous dust-enshrouded starbursts such as ULIRGs and sub-mm galaxies (e.g., Sanders et al. 1988; Dasyra et al. 2006; Alexander et al. 2008). Quantitatively, the observed *stellar* densities at radii $\sim 1 - 100$ pc in elliptical galaxies reach $\sim 20 \text{ g cm}^{-2}$ (Hopkins et al. 2010), implying $\tau \sim 100$ if a significant fraction of the stars were formed in a single gas-rich epoch. It is encouraging that this is within an order of magnitude of (and larger than!) the value of τ we find is required to explain the observed $M_{BH} - \sigma$ relation.

A fixed value of $\tau \sim 25$ independent of galaxy mass produces an $M_{BH} - \sigma$ relation with a slope and scatter in reasonable agreement with observations (see Fig. 9). Assessing the scatter more quantitatively will require a wider survey of merger orbits. We do find some tentative evidence for a shallower slope in the $M_{BH} - \sigma$ relation at the lowest galaxy masses, corresponding to $\sigma \lesssim 100 \text{ km s}^{-1}$. This range of masses is precisely where the observational situation is particularly unclear, with, e.g., possible differences between the BH-galaxy correlations in classical bulges and pseudo-bulges (Greene et al. 2008). It is also unclear whether major mergers are the dominant mechanism for BH growth in these lower mass galaxies (e.g., Younger et al. 2008).

Our simulations show that fragmentation of a galactic disk into clumps can be efficiently *induced* by a merger (e.g., Fig. 3), even when an isolated galaxy with same properties is Toomre stable (see, e.g., Wetzstein et al. 2007 for related ideas in the context of dwarf galaxy formation in tidal tails). As Figure 7 demonstrates, this fragmentation can produce a significant increase in star formation during the first close passage of galaxies even when there is little inflow of the diffuse ISM (because such inflow is suppressed by a bulge until later in the merger; Mihos & Hernquist 1996). In our simulations we often see a corresponding increase in the BH accretion rate due to the inspiral of dense gas-rich clumps (Fig. 3). The inflow of gas by this process may, however, be overestimated: stellar feedback not included in our simulations can unbind the gas in star clusters on a timescale of $\sim a \text{ Myr}$, returning most of the gas to the diffuse ISM (e.g., Murray et al. 2010; Hopkins & Quataert 2009).

Our calculations use subgrid sound speeds motivated by the observed turbulent velocities in galaxies (§2.2). We thus believe that our ISM model is physically well-motivated, even though the use of a subgrid sound speed necessarily introduces some uncertainty. Overall, the presence/absence of large-scale clumping of the ISM does not significantly change the final BH mass or the mass of new stars formed in our

simulations. It can, however, change the star formation rate and BH accretion rate as a function of time, particularly near the first close passage during a merger.

The tentative change in the $M_{BH} - \sigma$ relation we find for lower mass galaxies is largely due to our treatment of the ISM, rather than our BH feedback or accretion model. For a given gas fraction, lower mass galaxies have a lower gas surface density and thus the ISM is less prone to fragmentation (§3.4 and Fig. 8). Without the fragmentation after first passage, more gas is available to feed the BH at late times leading to somewhat higher BH mass (Fig. 10).

The BH accretion and feedback models used in this paper can be significantly improved in future work, allowing a more detailed comparison to observations. For example, Hopkins & Quataert (2009) carried out a large number of simulations of gas inflow in galactic nuclei from ~ 100 pc to $\lesssim 0.1$ pc (see, e.g., Levine et al. 2010 for related work). These can be used to provide a more accurate estimate of the BH accretion rate given conditions at larger radii in a galaxy (Hopkins & Quataert, in prep). Another important improvement would be to use a radiative transfer calculation to self-consistently determine the infrared radiation field produced by a central AGN (and distributed star formation). This could then be used to calculate the radiation pressure force on surrounding gas, eliminating the need for our parameterization of the force in terms of the optical depth τ .

ACKNOWLEDGMENTS

We thank Phil Hopkins and Yuval Birnboim for useful conversations. JD and EQ were supported in part by NASA grant NNG06GI68G and the David and Lucile Packard Foundation. Support for EQ was also provided in part by the Miller Institute for Basic Research in Science, University of California Berkeley. This research used resources of the National Energy Research Scientific Computing Center, which is supported by the Office of Science of the U.S. Department of Energy under Contract No. DE-AC02-05CH11231. This work was partially supported by the National Center for Supercomputing Applications under AST080048 and utilized the Intel 64 cluster Abe. The authors acknowledge the Texas Advanced Computing Center (TACC) at The University of Texas at Austin for providing HPC resources that have contributed to the research results reported within this paper.

REFERENCES

- Alexander D. M., Brandt W. N., Smail I., Swinbank A. M., Bauer F. E., Blain A. W., Chapman S. C., Coppin K. E. K., Ivison R. J., Menéndez-Delmestre K., 2008, *AJ*, 135, 1968
- Bondi H., 1952, *MNRAS*, 112, 195
- Booth C. M., Schaye J., 2009, *MNRAS*, 398, 53
- Chang C. A., Schiano A. V. R., Wolfe A. M., 1987, *ApJ*, 322, 180
- Ciotti L., Ostriker J. P., 1997, *ApJ*, 487, L105+
- Ciotti L., Ostriker J. P., Proga D., 2010, *ArXiv e-prints*
- Croton D. J., Springel V., White S. D. M., De Lucia G., Frenk C. S., Gao L., Jenkins A., Kauffmann G., Navarro J. F., Yoshida N., 2006, *MNRAS*, 365, 11

Dasyra K. M., Tacconi L. J., Davies R. I., Genzel R., Lutz D., Naab T., Sanders D. B., Veilleux S., Baker A. J., 2006, *New Astronomy Review*, 50, 720

DeBuhr J., Quataert E., Ma C., Hopkins P., 2009, *ArXiv e-prints*

Di Matteo T., Springel V., Hernquist L., 2005, *Nature*, 433, 604

Downes D., Solomon P. M., 1998, *ApJ*, 507, 615

Ferrarese L., Merritt D., 2000, *ApJ*, 539, L9

Gebhardt K., Bender R., Bower G., Dressler A., Faber S. M., Filippenko A. V., Green R., Grillmair C., Ho L. C., Kormendy J., Lauer T. R., Magorrian J., Pinkney J., Richstone D., Tremaine S., 2000, *ApJ*, 539, L13

Greene J. E., Ho L. C., Barth A. J., 2008, *ApJ*, 688, 159

Gültekin K., Richstone D. O., Gebhardt K., Lauer T. R., Tremaine S., Aller M. C., Bender R., Dressler A., Faber S. M., Filippenko A. V., Green R., Ho L. C., Kormendy J., Magorrian J., Pinkney J., Siopis C., 2009, *ApJ*, 698, 198

Häring N., Rix H., 2004, *ApJ*, 604, L89

Hernquist L., 1990, *ApJ*, 356, 359

Hernquist L., Mihos J. C., 1995, *ApJ*, 448, 41

Ho L. C., Darling J., Greene J. E., 2008, *ApJ*, 681, 128

Hopkins P. F., Hernquist L., Cox T. J., Di Matteo T., Martini P., Robertson B., Springel V., 2005, *ApJ*, 630, 705

Hopkins P. F., Hernquist L., Cox T. J., Robertson B., Krause E., 2007, *ApJ*, 669, 45

Hopkins P. F., Murray N., Quataert E., Thompson T. A., 2010, *MNRAS*, 401, L19

Hopkins P. F., Quataert E., 2009, *ArXiv e-prints*

Johansson P. H., Naab T., Burkert A., 2009, *ApJ*, 690, 802

Kawata D., Gibson B. K., 2005, *MNRAS*, 358, L16

King A., 2003, *ApJ*, 596, L27

Levine R., Gnedin N. Y., Hamilton A. J. S., 2010, *ArXiv e-prints*

McKee C. F., Ostriker J. P., 1977, *ApJ*, 218, 148

McNamara B. R., Nulsen P. E. J., 2007, *ARA&A*, 45, 117

Mihos J. C., Hernquist L., 1996, *ApJ*, 464, 641

Murray N., Quataert E., Thompson T. A., 2005, *ApJ*, 618, 569

Murray N., Quataert E., Thompson T. A., 2010, *ApJ*, 709, 191

Navarro J. F., Frenk C. S., White S. D. M., 1996, *ApJ*, 462, 563

Ostriker J. P., Choi E., Ciotti L., Novak G. S., Proga D., 2010, *ArXiv e-prints*

Price D. J., 2007, *Publications of the Astronomical Society of Australia*, 24, 159

Sanders D. B., Soifer B. T., Elias J. H., Madore B. F., Matthews K., Neugebauer G., Scoville N. Z., 1988, *ApJ*, 325, 74

Sazonov S. Y., Ostriker J. P., Ciotti L., Sunyaev R. A., 2005, *MNRAS*, 358, 168

Scannapieco E., Silk J., Bouwens R., 2005, *ApJ*, 635, L13

Shakura N. I., Sunyaev R. A., 1973, *A&A*, 24, 337

Sharma P., Quataert E., Stone J. M., 2007, *ApJ*, 671, 1696

Shen S., Mo H. J., White S. D. M., Blanton M. R., Kauffmann G., Voges W., Brinkmann J., Csabai I., 2003, *MNRAS*, 343, 978

Shlosman I., Begelman M. C., Frank J., 1990, *Nature*, 345, 679

Shlosman I., Frank J., Begelman M. C., 1989, *Nature*, 338, 45

Silk J., Rees M. J., 1998, *A&A*, 331, L1

Sironi L., Socrates A., 2010, *ApJ*, 710, 891

Springel V., 2005, *MNRAS*, 364, 1105

Springel V., Di Matteo T., Hernquist L., 2005a, *ApJ*, 620, L79

Springel V., Di Matteo T., Hernquist L., 2005b, *MNRAS*, 361, 776

Springel V., Hernquist L., 2003, *MNRAS*, 339, 289

Tabor G., Binney J., 1993, *MNRAS*, 263, 323

Tacconi L. J., Neri R., Chapman S. C., Genzel R., Smail I., Ivison R. J., Bertoldi F., Blain A., Cox P., Greve T., Omont A., 2006, *ApJ*, 640, 228

Vernaleo J. C., Reynolds C. S., 2006, *ApJ*, 645, 83

Wetzstein M., Naab T., Burkert A., 2007, *MNRAS*, 375, 805

Younger J. D., Hopkins P. F., Cox T. J., Hernquist L., 2008, *ApJ*, 686, 815

APPENDIX A: RESOLUTION STUDIES

In this section, we describe some of our resolution tests both with and without BH feedback. In the absence of feedback, the well-posed questions for resolution studies include both how the gas properties as a function of radius and time depend on the resolution and how integrated properties of the galaxy (e.g., the star formation rate) depend on resolution. However, the feedback, when present, has a nontrivial dependence on the resolution and it is by no means clear that the nonlinear system will in fact converge in a simple way with increasing resolution. Physically, e.g., the AGN's radiation pressure has the strongest effect on the gas that contributes the most to the optical depth, which is largely determined by the column density (the dust opacity being only a relatively weak function of temperature for the conditions of interest). Higher resolution simulations can resolve higher volume and column densities, largely at smaller radii close to the BH, and thus may change some of the details of the BH feedback. Indeed, Fig. 4 shows that the column density increases towards smaller radii in our simulations.

We first consider the question of how the nuclear gas properties depend on numerical resolution *in the absence of feedback*. To this end, the top left panel of Fig. A1 shows the BH accretion rate \dot{M}_{visc} calculated for three different particle numbers $N_p = 1.6 \times 10^5, 4.8 \times 10^5$, and 1.6×10^6 , with the gravitational force softening $\epsilon \propto N_p^{1/3}$.⁵ To make a fair comparison, the accretion rate is evaluated within a fixed volume ($R = 406$ pc) and for $\alpha = 0.05$ for all of the simulations. This choice corresponds to $R = 4\epsilon$ for the lowest resolution run, but is $R \simeq 8.6\epsilon$ for our fiducial resolution simulation. Fig. A1 shows that the lowest resolution simulation (red) does not adequately resolve the fragmentation of the gas, and the resulting peak in the accretion rate, near first passage. The medium and higher (= our fiducial) resolution simulations, however, agree reasonably well, except

⁵ In Fig. A1, \dot{M}_{visc} for the simulations without feedback (upper left) is calculated from the simulation snapshots and the accretion rate is not Eddington limited. The data outputs were relatively infrequent and attempting to integrate the BH mass over such large timesteps was inaccurate.

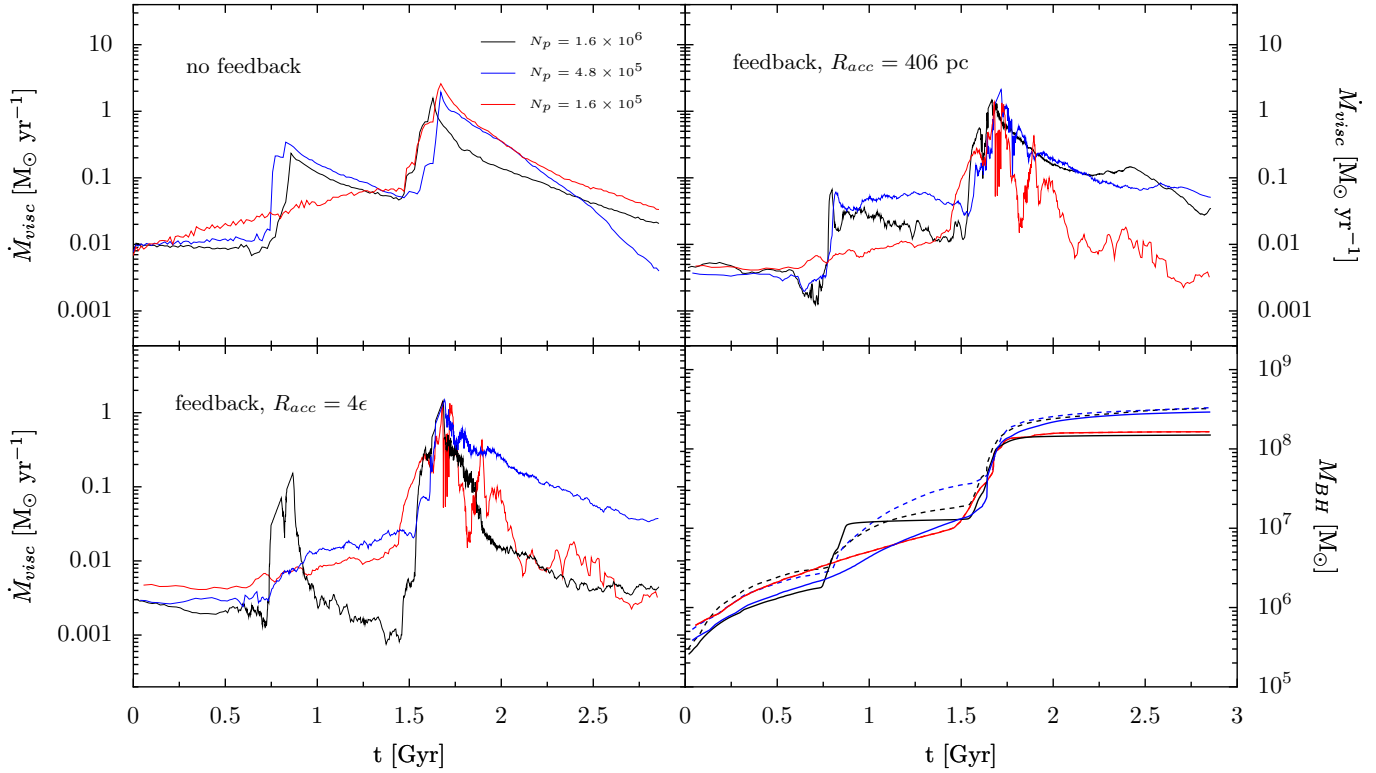


Figure A1. *Top left:* BH accretion rate for simulations without feedback at three resolutions (LRfidNof, MRfidNof, fidNof in red, blue and black respectively); \dot{M}_{visc} was computed for $\alpha = 0.05$ and using the same value of $R_{acc} = 406$ pc at all three resolutions (this corresponds to 4ϵ for the lowest resolution). *Top right:* BH accretion rate with feedback at the same three resolutions using $R_{acc} = 406$ pc. *Bottom left:* BH accretion rate with feedback at the same three resolutions using $R_{acc} = 4\epsilon$; here the accretion rate and feedback are calculated in different physical volumes at different resolutions. *Bottom right:* BH masses for all of the runs in this Figure with feedback. Solid lines are for $R_{acc} = 4\epsilon$ while dashed lines are for $R_{acc} = 406$ pc.

for a slight difference in the slope of $\dot{M}_{visc}(t)$ at late times. Computed over a larger spatial scale (\sim kpc), the agreement between these runs improves.

To assess the convergence in the presence of feedback, the top right panel of Fig. A1 shows the BH accretion rate \dot{M}_{visc} evaluated just as in the top left panel, i.e., using a fixed $R_{acc} = 406$ pc, in simulations with the same three particle numbers and force softening. Again the lowest resolution (red) simulation is clearly not adequate, but the medium (blue) and high (black) resolution simulations agree well; the integrated BH mass differs only by 2% in the latter two simulations.

As a final resolution test, the bottom left panel of Fig. A1 shows the BH accretion rate as a function of time in simulations with the same three resolutions and force softening, but in which $R_{acc} = 4\epsilon$. Thus in this case the accretion rate is determined, and the feedback applied, on increasingly small spatial scales in the higher resolution simulations. This is probably the most physically realistic (see §2.4). This panel shows that the large peak of accretion at final coalescence ($t \sim 1.8$ Gyr) is quite similar in all three cases. This is set by the physics of feedback by momentum deposition and is a robust property of all of our simulations. A corollary of this is that the final BH mass, as shown in the bottom right panel of Fig. A1, is the same to within a factor of ~ 2 for the three different resolutions. However, the results in the lower left panel of Fig. A1 also clearly demon-

strate that the detailed evolution of the accretion rate is sensitive to the resolution. This is not particularly surprising: at fixed resolution, Fig. 5 has already demonstrated that the details of $\dot{M}_{visc}(t)$ depend on the value of R_{acc} – although, again, neither the integrated BH mass or star formation rate do. One implication of these results is that it is difficult for current simulations of BH growth to make quantitative predictions about the light curves of AGN activity triggered by mergers.

APPENDIX B: CODE VERIFICATION

We have tested our modifications to GADGET on a number of simplified problems that have answers that can be easily obtained through other methods. §B1 describes tests of the additional momentum feedback force applied to a thin spherical shell of gas. §B2 describes tests in which the force is applied to the gas particles in the central regions of an isothermal sphere. Two ways of implementing the force are tested: to a fixed number of particles around the BH, and to all particles within a fixed region R_{acc} around the BH.

As we are concerned with the performance of our BH accretion and feedback model, in all of the tests presented in this appendix, the multiphase equation of state and star formation model of Springel & Hernquist (2003) are *not* used; instead we use an adiabatic equation of state with $\gamma = 5/3$.

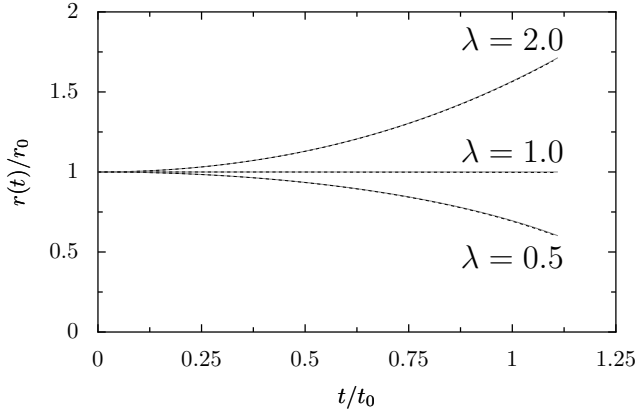


Figure B1. Time evolution of the radius of the test shell for three values of radiation force: $\lambda = 0.5, 1.0, 2.0$ (dashed curves). The results match closely with the solutions from integrating eq. (B2) (superposed grey curves). Here the force is applied to the 25000 innermost gas particles of the 5×10^4 that make up the shell. Time is in units of $t_0 = \sqrt{r_0^3/GM_{BH}}$ and the radius is in units of r_0 , where r_0 is the initial radius of the gas shell.

B1 Gas shells

To test that the code is applying the radiation pressure force in equation (7) correctly, we have run the code for a simple system containing a black hole particle with a large mass and a thin spherical shell of gas with negligible temperature, pressure and mass. As this gas resides in a thin shell, this problem is more well-posed if we apply the radiation force to a fixed number, N , of gas particles.

This system has a critical luminosity defined by the point at which the radiation force balances the inward pull of gravity. As the gas shell is of low temperature and pressure, we can ignore pressure forces. For a black hole of mass M_{BH} and a gas shell of mass m at a radius r_0 the critical luminosity L_C satisfies (we take $\tau = 1$ for simplicity)

$$L_C = G \frac{M_{BH} m}{r_0^2} c. \quad (B1)$$

When the luminosity is set to this value, the gas shell should experience no net force. For other values of the luminosity, the expected behaviour can easily be calculated by noting that the gas shell, in the absence of any pressure forces, should have a radius, $r(t)$, that satisfies

$$m \frac{d^2 r(t)}{dt^2} = - \frac{GM_{BH} m}{r(t)^2} + \frac{L}{c}. \quad (B2)$$

This is easily integrated to give the expected behavior of the gas shell.

A number of tests of this system were performed with varying luminosities, parameterized by the ratio of the luminosity applied to the critical luminosity,

$$\lambda = \frac{L}{L_C}. \quad (B3)$$

Fig. B1 shows the exact result in grey, with the numerical solution from the modified version of GADGET in black, for runs with $\lambda = 0.5, 1.0$ and 2.0 . For these tests the number of particles in the shell is $N_{shell} = 50000$, and the force was applied to $N = 25000$ of them. In all cases, the numerical

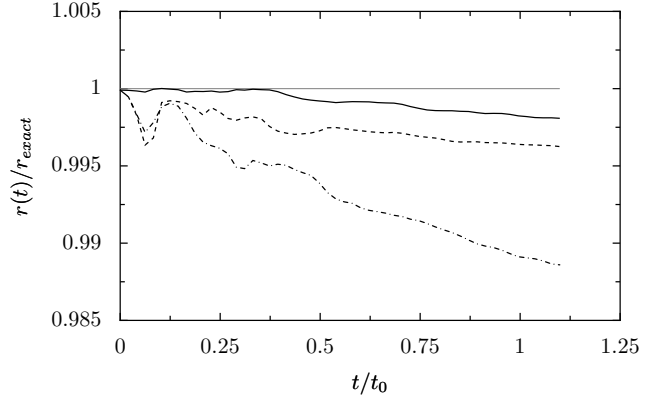


Figure B2. Time evolution of the radius of the test shell for three values of N/N_{shell} : 0.5 (solid), 0.25 (dashed), and 0.1 (dot-dashed). The numerical solutions are normalized by the exact solution from eq. (B2). The radiation force is fixed to be $\lambda = 2.0$. The radius $r(t)$ changes by only about 1% as N is changed, indicating that our results are insensitive to the exact number of particles to which the radiation force is applied.

solution appears indistinguishable from the exact solution of eq. (B2).

We have also tested the dependence of the results on the value of N/N_{shell} , the fraction of particles that receives the radiation force. Fig. B2 shows the ratio of the numerical solution from our code to the exact solution for $N/N_{shell} = 0.5, 0.25$, and 0.1 for the $\lambda = 2.0$ model. This demonstrates that even though the magnitude of the force on an individual particle increases as N decreases, the overall dynamics of the shell is the same, with the radii differing by only $\sim 1\%$ in the three cases. This is primarily due to the fact that the SPH particles are collisional and can thus transfer their motion to their neighbors via pressure forces. The extra momentum imparted to the subset of particles is transferred in part to the outer region of the shell, leading to the overall motion that agrees well with the exact solution. By extension, if N were to vary over the duration of the simulation, the results would also not depend strongly on the particular value.

B2 Isothermal Sphere

We have performed a second set of tests of the feedback model using an isothermal background given by a King model. The mass of the system is split into two parts. The bulk of the mass makes up the collisionless background that is drawn from the full phase space distribution of the King model. A small fraction of the mass, $f_g = 0.05$, is assigned as collisional SPH particles. These gas particles follow the same spatial profile as the collisionless background but are given zero initial velocities and a very low temperature. Both components are realized with 10^5 particles. Finally, a black hole particle with a small mass is placed at rest at the center of the distribution.

In the absence of feedback, the SPH particles are not in equilibrium by construction and should flow toward the center of the potential provided by the collisionless background. When the feedback is switched on in the isothermal King potential near the center, the feedback will again have a critical value set by force balance:

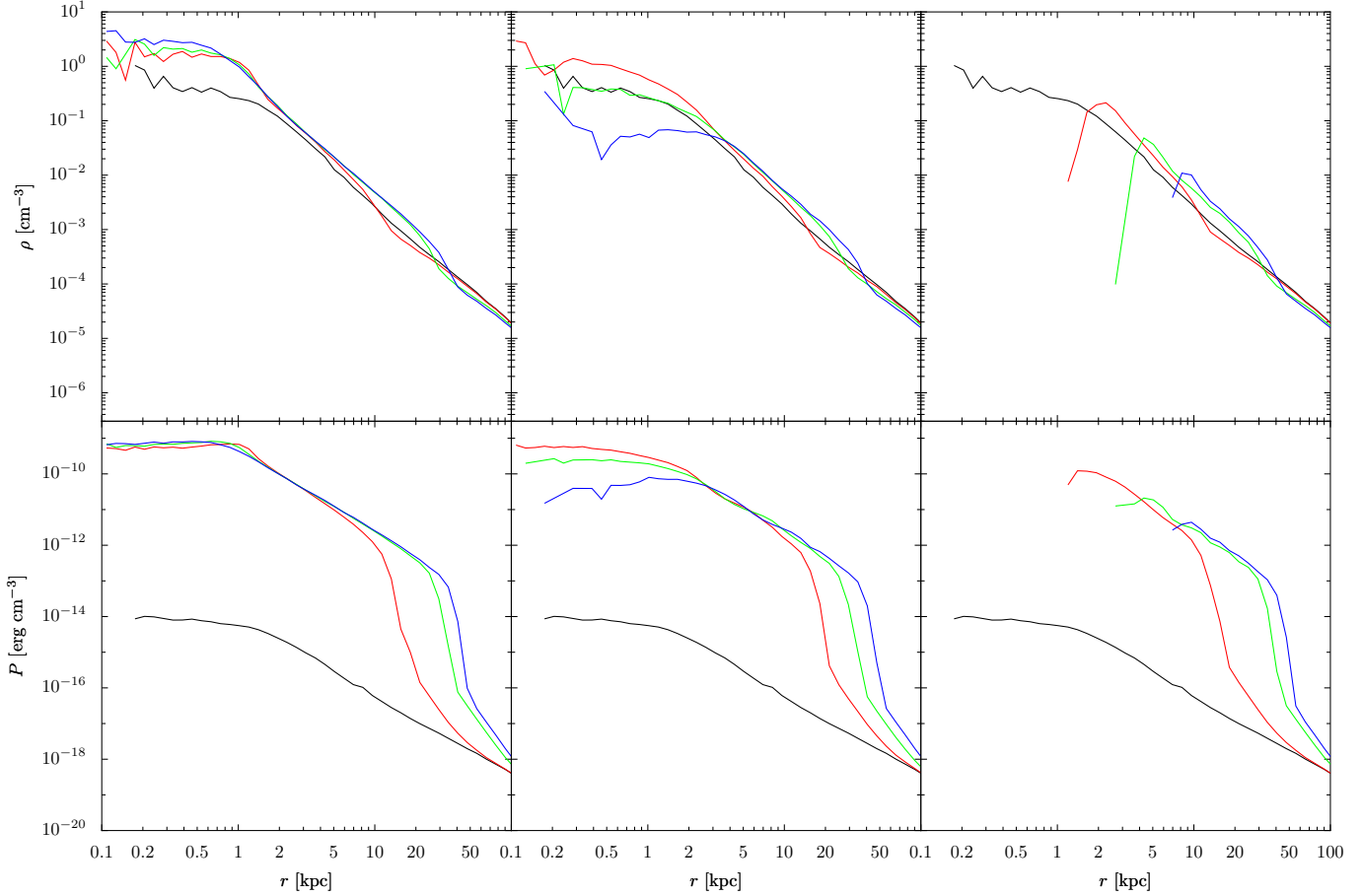


Figure B3. The density (top) and pressure profiles (bottom) in simulations of an isothermal sphere of gas embedded in an isothermal King potential. Three different simulations are shown: without feedback from a central black hole, $\lambda = 0.0$ (left), $\lambda = 1.0$ (middle) and $\lambda = 2.0$ (right). Each simulation is shown at four times: the initial profile (black) and $t = 0.16$ (red), 0.32 (green), 0.48 (blue) Gyr.

$$\frac{L_c}{c} = 4 \frac{f_g \sigma^4}{G}. \quad (\text{B4})$$

When the luminosity is below this value, we expect the extra momentum to be insufficient to clear the gas out of the center. When the luminosity exceeds this value, the feedback should be strong enough to clear the central regions of the distribution. To test this, we apply feedback with a constant luminosity. Again, we parameterize the strength of the feedback as $\lambda = L/L_c$.

We have tested two ways of assigning the radiation force. In the first case, the force is shared (equally) by a fixed number of gas particles nearest to the black hole. In the second case, the force is shared by all gas particles within a fixed radius of the black hole. We discuss the results separately below.

B2.1 Fixed N

For the tests in this subsection, the radiation force is applied to a fixed number of gas particles: $N = 500$. The King model has $\sigma = 100 \text{ km s}^{-1}$, $\Psi/\sigma^2 = 12$ and a total mass of $10^{12} M_\odot$.

Fig. B3 compare the density and pressure profiles of three runs with $\lambda = 0$ (i.e. no feedback; left panels), 1 (middle), and 2 (right). Four timesteps are shown: $t = 0$ (black), 0.16 (red), 0.32 (green), and 0.48 Gyr (blue). As expected,

the gas flows to the center in the absence of feedback, increasing the density and pressure as the gas begins to equilibrate in the background potential. The middle and right panels show that the feedback clearly has an effect on the gas at the center, providing some support for the incoming gas, allowing the gas to have a lower pressure. For the case with $\lambda = 2$, the feedback is strong enough to effectively clear out the central region.

The nature of the feedback allows a calculation of how the size of the evacuated region should grow with time. Ignoring the thickness of the shell swept up as matter begins to be driven out by the feedback, momentum conservation gives

$$\frac{d}{dt} [M_{shell}(r) dr/dt] = \frac{L}{c} - \frac{GM_{bg}(r)M_{shell}(r)}{r^2} \quad (\text{B5})$$

where $M_{shell}(r)$ is the initial mass distribution of gas and $M_{bg}(r)$ is the mass distribution of the background. Near the center of the initial distribution, both the gas and background have an isothermal distribution, for which the mass increases linearly with the distance from the centre. This makes the right hand side of Eq. (B5) a constant. In this case, the size of the evacuated region, $r(t)$, depends linearly on time:

$$r(t) = \sqrt{2(\lambda - 1)(1 - f_g)\sigma t} + C \quad (\text{B6})$$

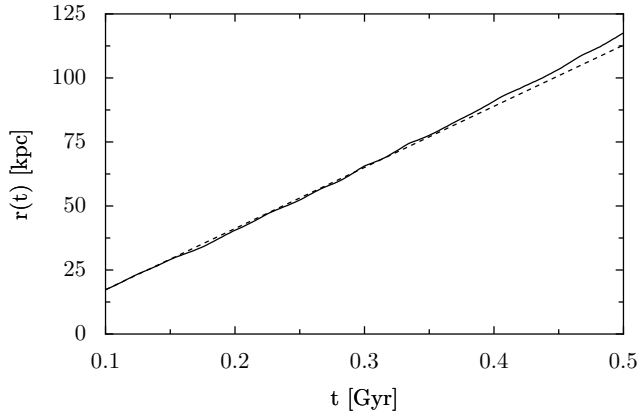


Figure B4. Time evolution of the size of the evacuated region for the isothermal sphere test. The $\lambda = 4$ simulation results shown (solid) match well with the analytic solution (Eq. B6; dashed).

where C is a constant of integration to account for the finite time required to form the shell of swept up gas.

Fig. B4 shows the size of the evacuated region as a function of simulation time for a run with $\lambda = 4$, and the exact solution for a shell moving in an isothermal background (Eq. B6) with C chosen to match the position of the shell at $t = 0.1$ Gyr. The size of the evacuated region is defined by the position of the gas particle closest to the black hole. The agreement is very good with only slight deviation at the latest times. For the model employed, the potential is only isothermal near the origin, so when the shell expands sufficiently, the potential shallows and the shell should move faster than the prediction. This is indeed seen at late time in Fig. B4.

B2.2 Fixed R_{acc}

For the galaxy merger simulations, we apply the force inside a fixed R_{acc} throughout the simulation. In this section, we run a similar set of tests as in the previous subsection but we hold R_{acc} fixed. When the number of particles inside R_{acc} becomes small, however, the feedback force exerted on individual particles becomes spuriously large. We therefore impose an additional condition of minimum N on the feedback. For the tests in this subsection, the feedback is applied to those particles inside R_{acc} , or to the innermost 100 gas particles if there are fewer than this inside R_{acc} . For the simulations in the main paper, however, there were always enough particles inside the accretion and feedback region to avoid the need for such a lower bound on N .

Our first test uses a constant $L = 4L_c$, and holds R_{acc} fixed. We use a King model as in the previous section, but with slightly different parameters to connect more closely to our fiducial simulation: $\sigma = 160 \text{ km s}^{-1}$, $\Psi/\sigma^2 = 12$ and a total mass of $10^{12} M_\odot$. We tested this model for three different sizes of the accretion and feedback region: $R_{acc} = 0.7, 1.4$ and 2.8 kpc. The smallest region has initially $N \sim 500$. Note that the values of R_{acc} used here are larger than those used in our galaxy merger simulations in the main text. These values of R_{acc} were necessary to ensure that R_{acc} contains a reasonable number of particles. In the galaxy merger calculations, the overall larger number of particles in the simulation and the high gas density in the central regions

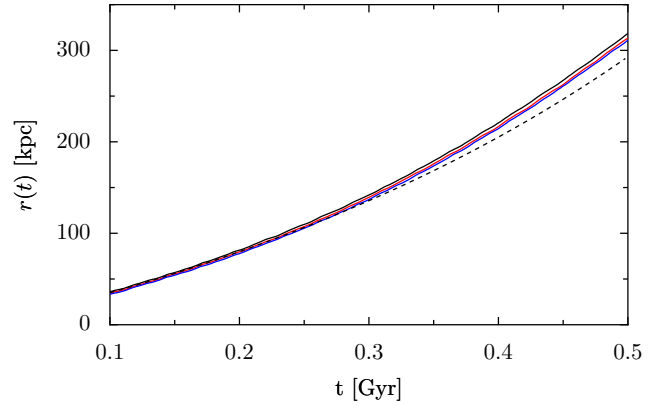


Figure B5. Radius of the swept up shell for the isothermal sphere test with $\lambda = 4$ and fixed R_{acc} : 0.7 (black), 1.4 (red), and 2.8 kpc (blue). To avoid numerical problems, the feedback was always applied to at least $N \sim 100$ particles. The numerical results agree well with the dashed curve, which shows a numerical integration of the analytic equation for the shell radius (eq. B5).

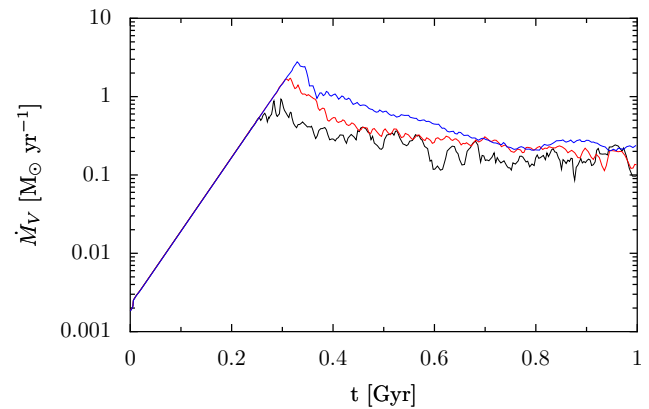


Figure B6. The black hole accretion rate for isothermal sphere simulations in which the full black hole accretion and feedback model are used ($\alpha = 0.1$ and $\tau = 1$). Three different values of R_{acc} are shown: $R_{acc} = 0.7$ (black), 1.4 (red), and 2.8 kpc (blue). All three agree well with each other.

imply that smaller values of R_{acc} can be reliably used. They are also more physical, as we argued in §2.4.

Fig. B5 shows the position of the shell of swept up material for the three runs with $R_{acc} = 0.7, 1.4$ and 2.8 kpc in black, red and blue respectively. Initially, all the gas inside R_{acc} experiences the extra force. As the region becomes more evacuated and the number of particles inside R_{acc} drops, we transition to applying the force to the $N = 100$ particles closest to the BH. The evolution of the shells in this case is quite similar to the evolution in the last section. The model used in this section is smaller in size and so the shell expands past the isothermal core of the King model earlier. As a result, it begins to accelerate outward sooner. However, the tests with different R_{acc} have essentially identical evolution.

Finally, we run a test in which we determine the luminosity from the accretion rate as in Eq. (7), and increase the BH mass in time accordingly. This test thus employs the full feedback and accretion model of our galaxy merger

simulations. We use the same $\sigma = 160 \text{ km s}^{-1}$ King model, and took $\alpha = 0.1$ and $\tau = 1$ for the feedback parameters. The initial mass of the black hole was $M_{BH,i} = 10^5 M_\odot$.

Fig. B6 shows the accretion history of the BH for the runs with $R_{acc} = 0.7, 1.4$, and 2.8 kpc . In each test, the feedback is initially Eddington limited and it is not until about $t = 0.3 \text{ Gyr}$ that the luminosity approaches that required to evacuate the gas out of R_{acc} . At this point, the gas begins to move out of R_{acc} and form a shell of material at $R \sim R_{acc}$. This shell then remains fairly steady as the accretion rate self-regulates around the critical luminosity. As the three values of R_{acc} are all inside the isothermal core of the King model, the critical luminosities (eq. B4) are the same, and we would thus expect the accretion rate to self-adjust to the same value at late times. This is indeed borne out in the simulations shown in Fig. B6. Of these three runs, only the calculation with $R_{acc} = 0.7 \text{ kpc}$ spends a significant amount of time with fewer than 100 particles inside R_{acc} . Despite the large change in the size of the feedback region, Fig. B6 shows that the evolution of the gas is quite similar. The black hole masses for these three runs differ by only a factor of ~ 2 at the end of the simulation.